Master's thesis

NTNU
Norwegian University of Science and Technology
Faculty of Natural Sciences
Department of Chemistry

Jostein Rossvoll

Extracting Dynamical Information from Complex Systems using Advanced Path Sampling Techniques

Master's thesis in Applied Theoretical Chemistry
Supervisor: Titus Sebastiaan van Erp
Co-supervisor: Anders Lervik
May 2022

NTNU
Kunnskap for en bedre verden

Jostein Rossvoll

Extracting Dynamical Information from Complex Systems using Advanced Path Sampling Techniques

Master's thesis in Applied Theoretical Chemistry
Supervisor: Titus Sebastiaan van Erp
Co-supervisor: Anders Lervik
May 2022

Norwegian University of Science and Technology
Faculty of Natural Sciences
Department of Chemistry

NTNU
Kunnskap for en bedre verden

Abstract

Computer based simulation techniques are becoming ever more important as both a substitution and compliment to experimental research, since they are less costly and can provide microscopical dynamical information which otherwise is unattainable. Of particular interest are path sampling techniques such as TIS and more recently RETIS, which promises ever faster attainment of dynamical information such as rate constants. It is therefore of importance to further develop these methods with new moves to decrease cost and improve upon results. The wire fencing move is a new move under development which was tested out on a system of cadmium selenide crystals. Cadmium selenide nanocrystals are under development as a nanostructured semiconductor in several applications. Such crystals possess two stable structures, wurtzite and rocksalt as well as a metastable h-MgO structure. By utilising molecular dynamics and path sampling, we found that a 2048 atom CdSe crystal produced a plane defect which lowered the transition pressure between the wurtzite and rocksalt structure from 11 GPa in a perfect crystal to 9 GPa. Pressure was found to be the driving factor facilitating transition. The wire fencing move was found to raise the acceptance rate of trajectories but provided an overall higher simulation time than conventional moves.

Sammendrag

Databaserte simuleringsteknikker spiller en gradvis større rolle som både en erstatning og en utfyllende rolle til eksperimentell forskning, siden disse teknikkene er mindre kostbare og kan gi mikroskopisk dynamisk informasjon. Av spesiell interesse er path samplingteknikker som TIS og nyligere RETIS, som lover raskere anskaffelse av dynamisk informasjon som ratekonstanter. Det er derfor viktig å videre utvikle disse metodene med nye "movesfor å senke kostnaden og forbedre resultater. "Wire fencinger en ny "move"under utvikling som ble testet ut på et system bestående av kadmium selen krystaller. Kadmium selen nanokrystaller er under utvikling og forskning nanostrukturerte halvledere i flere applikasjoner. Disse krystallene har to stabile strukturer, wurtzite og rocksalt i tillegg til en metastabil h-MgO struktur. Gjennom molekylær dynamikk og path samplingble det funnet at en 2048 atom CdSe krystall produserte en planar defekt som senket overgangstrykket mellom wurtzite og rocksalt fra 11 GPa i en perfekt krystall til 9 GPa. Trykket ble identifisert som primærfaktoren i overgangen. "Wire fencing"økte akseptansraten til simuleringene men ga en lengre simuleringstid enn konvensjonelle teknikker.

Table of Contents

1 Background & motivation **5**

2 Theory **6**

2.1 Rare events 6

2.2 Molecular Dynamics 7

2.3 Monte Carlo 9

2.3.1 Importance Sampling 10

2.3.2 The Metropolis method 10

2.4 Path Sampling 12

2.4.1 Transition State Theory 12

2.4.2 Order Parameters & Reaction Coordinates 13

2.4.3 Transition Path Ensemble 14

2.4.4 Deterministic Dynamics 15

2.4.5 Stochastic Dynamics 16

2.5 Sampling procedure 16

2.5.1 Detailed Balance 17

2.5.2 Shooting moves 17

2.5.3 Deterministic considerations 19

2.5.4 Stochastic Considerations 19

2.6 Rate computation 20

2.6.1 Time correlation function 20

2.6.2 Umbrella Sampling 21

2.7 Transition Interface Sampling 21

2.8 Replica Exchange Transition Interface Sampling 24

2.9 Wire fencing 25

2.10 CdSe Nanocrystals 26

3 Experimental **28**

3.1 Molecular Dynamics initialisation 28

3.2 Initial path creation 28

3.3 RETIS settings 29

4 Results & Discussion **30**

4.1 Molecular Dynamics 30

4.1.1 Crystal defects & structure 30

4.1.2 Pressure and Temperature effects 31
4.1.3 Total energy 33
4.1.4 Transition 35
4.2 Rare events 36
4.2.1 Initial trajectory issues 36
4.2.2 Energy switching 37
4.2.3 Interface placement 38
4.2.4 Wire fencing 39
4.2.5 Crossing probabilities 40

5 Conclusion **41**

6 Further development **41**

7 Acknowledgements **41**

Nomenclature

λ	Order Parameter
τ_{mol}	Time regime of molecular fluctuations inside stable state
τ_{rxn}	Time regime of a rare event reaction
f_A	Initial Flux
A, **B**	Overall state A and B
A, B	Stable state A and B
CdSe	Cadmium Selenide
DFC	Defect Free Crystal
MC	Monte Carlo
MD	Molecular Dynamics
OP	Order Parameter
PDC	Plane Defected Crystal
RC	Reaction Coordinate
RETIS	Replica Exchange Transition Interface Sampling
TIS	Transition Interface Sampling
TPS	Transition Path Sampling
TS	Transition State
TST	Transition State Theory

1 Background & motivation

Computer based simulation techniques have been devised to be both an alternative to and complement traditional experiments. Broadly speaking, there are two main classical methods one can use to study a system. These methods are Molecular Dynamics (MD) and Monte Carlo (MC) approaches. MD is a dynamical method where the equations of motion are integrated for every atom in the system to model their time evolution. The interactions between atoms are modeled by a force field which often has to be system specific to accurately describe the time evolution. Usually, an MD simulation is ran on the timescale of microseconds to milliseconds with the fastest high power computers available today. If we want to model something that rarely happens on this timescale, but is readily available at experimental timescales which range from minutes to hours, we will undoubtedly run into problems. This is what is known as a rare event and is a problem which MD is unsuited to handle. For that, we turn to MC. Broadly speaking, MC implements trial moves, which alters the system to explore its configuration space. The advantage of this method is that the alteration does not need to be dynamical in nature, allowing it to surpass energy barriers. Naturally, this means that MC does not provide any dynamical information, only thermodynamic information.

Advanced techniques for studying rare events have been developed and improved since the 1950's. Major methods for sampling dynamical trajectories of rare events include the Bennett-Chandler (BC) approach [5, 6] and Transition Path Sampling (TPS) [33, 38]. In the BC approach, a single transition state has to be identified from which fleeting trajectories would be initiated from to create reactive trajectories. TPS on the other hand allows trajectories to proceed through several different routes, making it more useful when there are more than a single transition state. TPS combines both MC and MD by altering a phase space point with a trial move, and then generating a full dynamical trajectory from that point with MD. This circumvents the issue of MD not creating a reactive trajectory due to the time scale, and we get dynamical trajectories unlike standard MC. Further development of the TPS method yielded Transition Interface Sampling (TIS)[37] and more recently Replica Exchange TIS (RETIS)[48] which built upon the original framework of TPS, but added a set of hypersurfaces in phase space between stable state A and B which turned the probability of reaching state B given that a trajectory started in state A into a problem of conditional crossing probabilities between the interfaces. Path sampling methods have grown ever more efficient by introducing various methods of calculating rate constants and new trial moves which facilitate ergodic sampling of phase space. In addition, these methods provide valuable insight into the mechanisms of transition which can be nearly impossible to determine experimentally. Therefore, path sampling techniques should be further developed to limit the computational cost of running a simulation. One of these developments is the new "wire fencing" move. One of the goals of this thesis is to test this move on a realistic complex system and compare it with established moves in terms of cost and precision.

To illustrate how path sampling techniques can be utilised to extract dynamical information from systems, nanocrystals of cadmium selenide (CdSe) was chosen as the system to study. CdSe has been studied extensively since it exhibits promising features as a nanostructured semiconductor in applications such as solar cells, light-emitting diodes and biological imaging [16, 21, 39]. Under pressure, the 4-coordinated hexagonal wurtzite structure of the crystal transitions into a 6-coordinated rocksalt structure. Due to wide disparity in timescale between experimental and computational conditions, the pressure needed to induce a transition in the range of nanoseconds in vastly higher than the pressure needed at experimental conditions. This leads to trajectories that exhibit aggressive, disruptive transitions with multiple nucleation centers[43]. In addition, computational experiments have found that an intermediate 5-coordinated h-MgO structure can be observed in nanocrystals, but is energetically unavailable in bulk crystals. To accurately study the transition between all three structures with pressures that resemble experimental conditions, we turn to path sampling methods as a way of obtaining dynamical information about the system that cannot be found experimentally. Path sampling plays a vital role in getting a detailed understanding of atomistic pathways which are crucial if we are to stabilise metastable structures by controlling crystal shape and surface configuration, which is a technological challenge [43]. This thesis will utilise the methods outlined above to study the mechanics and kinetics with both defect free crystals and crystals with realistic defects.

2 Theory

The theory section begins with a description of rare events and the issue they present when studying systems with computer simulation. Following this, Molecular Dynamics and Monte Carlo methods are described as a precursor for discussing path sampling which combines both methods for ease of sampling. Next, techniques that build on the framework of path sampling are discussed as well as the new wire fencing move before discussing the structure and properties of cadmium selenide nanocrystals.

2.1 Rare events

A rare event is an event occurring with a very small probability. Defining small is dependent on the application domain the rare event is occurring in [42]. If the system of interest is a molecular system simulated with MD for instance, a rare event could be any transition that we can observe under experimental conditions quite easily, but remain elusive in a simulation. Examples of rare events within molecular simulations include protein folding, conformational changes of molecules, cluster isomerisations, chemical reactions, solid-solid phase transitions etc.[46]. Depending on the complexity of the forcefields used in an MD simulation, systems of anywhere between 100 - 100 000 molecules can be simulated for a period of microseconds to milliseconds [46]. This time regime is usually not sufficient to simulate a rare event at experimental conditions. Figure 1 shows the oxidation of carbon monoxide to create carbon dioxide. The reaction takes place over the timescale of -10^7 seconds which is equal to 100 nanoseconds which can be a costly system to simulate.

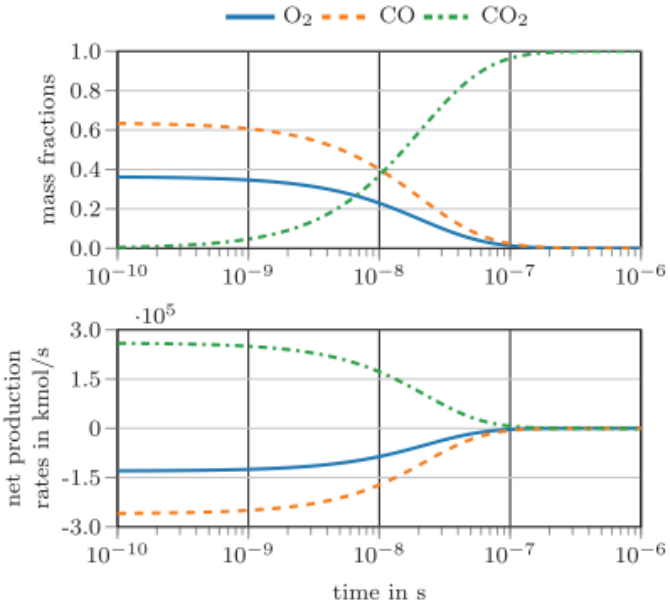

Figure 1: Oxidation reaction of carbon monoxide to produce carbon dioxide. The upper figure shows the mass fractions of each compound and the lower figure shows the net production rate. Figure from [51].

A system will transition into the state where the Gibbs free energy is the lowest given enough time. The Gibbs free energy $G = H - TS$ where H is the enthalpy, T is the temperature and S is the entropy. In cases where the reactant and product state are similar, the change in entropy will be not be significant, and thus it is the enthalpy that determines the most stable state. Enthalpy can be expressed as $H = U + pV$ where U is the internal energy and pV is the pressure-volume energy term.

The reason why these occurrences are so inaccessible by MD is due to the separation of timescales. For rare events, there are two time regimes we need to consider, τ_{mol} and τ_{rxn} with $\tau_{mol} < \tau_{rxn}$ which are the molecular relaxation timescale and the reaction timescale, respectively [48]. τ_{mol}

is the time regime where molecular fluctuations can be observed within a particular stable state, but this time regime is too short to observe a rare event. τ_{rxn} on the other hand is a longer time regime where the chance of observing a rare event is drastically larger. The exact range of values for both of these regimes are system dependent.

Therefore, many activated processes cannot be studied using brute-force MD because the probability to observe a reactive event within reasonable CPU time is practically zero [46]. To understand why a brute-force MD simulation has difficulties simulating a rare event, consider figure 2. Here, the reactant and product state of a chemical reaction are separated by a potential energy barrier. Since the product state has a lower potential energy than the reactant state, it is expected that over time most molecules will end up in the product state. However, over a short timescale, the system will linger in the reactant state because it is energetically unfavourable for the system to traverse the potential energy barrier.

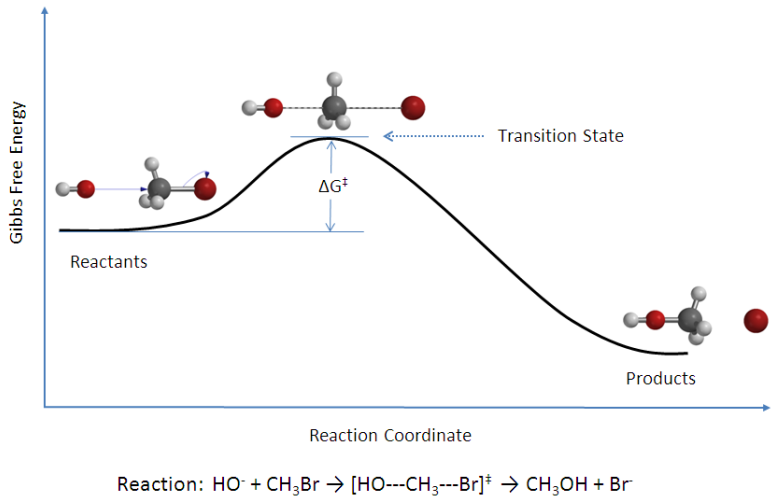

Figure 2: Reaction coordinate against Gibbs free energy for the bimolecular reaction between bromomethane and a hydroxide anion. Figure from [52].

2.2 Molecular Dynamics

Molecular Dynamics (MD) is a computational technique wherein the goal is to accurately describe the time evolution of a system. This is done through integration of Newton's laws of motion. These three laws are formulated as such[28]:

1. A body continues to move in a straight line at a constant velocity unless a force acts upon it.
2. Force equals the rate of change of momentum.
3. To every action there is an equal and opposite reaction.

Note that the third point does not hold unless the forcefield consists of pair potentials. A dynamical trajectory, which is a sequence of configurations evolving in time according to the forces acting on it, is made by solving the differential equations encapsulated by Newton's second law ($F = ma$) where F is the force, m is the mass and a is the acceleration

$$\frac{d^2 x_i}{dt^2} = \frac{F_{x_i}}{m_i} \tag{1}$$

The implication of Newton's second law is that acceleration is determined by $a = F/m$ with $F = - \bigtriangledown V$ where V is the potential energy. V is determined by the configuration r since the electrostatic interactions that give rise to potential energy can be determined through r. This means that accelerations are determined via configurations, unlike velocities which are independent to configuration[28].

(1) provides us with the motion of a particle with mass m_i along the x_i coordinate where F_{x_i} is the force working on the particle in the direction of x_i. By applying these dynamics to MD, we have what is known as Newtonian dynamics describing our system. Newtonian dynamics are deterministic in nature, meaning that the initial conditions of the system fully determine the overall trajectory. This is opposed to stochastic dynamics, where several trajectories initiated with the same initial conditions might still create several different dynamical trajectories. Note that many baro- and thermostats used in MD simulations possess stochastic elements. There are several different types of systems in which Newtonian dynamics are applied. First being a system where no force is being applied to the particles between collisions of the particles. Then, each particles time evolution can be described by $\nu_i \delta t$ where ν_i is the velocity of the particle after collision and δt is the time between collisions. Next, we can consider a system where the particles between collisions have a constant potential act upon them. Lastly, and most difficult, is the system where the potential on each particle is dependent upon the position of a particle relative to the other particles within a cutoff distance for modelling interparticle interactions[28]. To relieve this problem, several types of *force fields* have been devised which often are system-specific, but excel at modelling the interactions between particles for efficient MD simulations.

In a realistic model, the positions r and velocities ν of a particle at a certain timestep t is determined by the forces acting on it through the intermolecular potential of every other particle within a certain cutoff distance. This gives rise to a continuous potential, which means the motion of particles are coupled, leading to a many-body problem which cannot be solved analytically. This also leads to the question of how to integrate the equations of motion. For this we turn to *finite difference methods* [28]. The assumption in these methods is that the continuous potentials are pairwise additive. The methods then base themselves on the idea that integration can be divided into steps separated in time by a fixed timestep δt. The total force that acts on a given particle at time t is then determined as the vector sum of its interactions with the other particles within the cutoff distance [28]. The force then allows us to calculate accelerations and thus velocities at time t so that we can determine positions and velocities at $t + \delta t$. Several algorithms exist that can integrate the equations of motion within the finite difference framework. The method relies on all properties we wish to calculate can be approximated as a Taylor series expansion [28]

$$r(t + \delta t) = r(t) + \delta\nu(t) + \frac{1}{2}\delta t^2 a(t) + \frac{1}{6}\delta t^3 b(t) + \frac{1}{24}\delta t^4 c(t) + ... \tag{2}$$

$$\nu(t + \delta t) = \nu(t) + \delta t a(t) + \frac{1}{2}\delta t^2 b(t) + \frac{1}{6}\delta t^3 c(t) + ... \tag{3}$$

$$a(t + \delta t) = a(t) + \delta t b(t) + \frac{1}{2}\delta t^2 c(t) + ... \tag{4}$$

$$b(t + \delta t) = b(t) + \delta t c(t) + ... \tag{5}$$

$\nu(t)$ is here the velocity (first derivative of position with respect to time), a is the acceleration (second derivative), b is the third derivative and c is the fourth derivative and so on. The Verlet method [4] is an early scheme for integrating the equations of motion [28]. This algorithm uses both position and acceleration at t as well as the positions from previous step $t - \delta t$ to determine positions at the next time step $t + \delta t$. The following relations can be written down as

$$r(t + \delta t) = r(t) + \delta t\nu(t) + \frac{1}{2}\delta t^2 a(t) + ... \tag{6}$$

$$r(t - \delta t) = r(t) - \delta t\nu(t) + \frac{1}{2}\delta t^2 a(t) - ... \tag{7}$$

By adding both of these together we get

$$r(t + \delta t) = 2r(t) - r(t - \delta t) + \delta t^2 a(t) \tag{8}$$

There is no explicit mention of the velocities in the Verlet algorithm, but they can be calculated by division of the difference in positions at $t + \delta t$ and $t - \delta t$ by $2\delta t$

$$\nu(t) = [r(t+\delta t) - r(t-\delta t)]/2\delta t \tag{9}$$

The disadvantages of the Verlet algorithm is that positions are acquired by adding a small term ($\delta t^2 a(t)$) to the difference two of much larger terms ($2r(t)$ and $r(t-\delta t)$). This often leads to a loss of precision [28]. Another issue is the lack of velocities in the computation of positions, leading to velocities not being available until positions have been determined at the next time step. The algorithm is also not self-starting since the new positions are acquired from both current and previous positions. When $t = 0$ there is only one set of positions, so the previous positions has to be obtained by some other scheme, such as using the Taylor series expansion and truncating after the first term[28].

The integrator used in this thesis is the *velocity Verlet method*[9]. This method has the distinct advantage that it can provide both positions, velocities and accelerations without compromising precision

$$r(t+\delta t) = r(t) + \delta t\nu(t) + \frac{1}{2}\delta t^2 a(t) \tag{10}$$

$$\nu(t+\delta t) = \nu(t) + \frac{1}{2}\delta t[a(t) + a(t+\delta t)] \tag{11}$$

The implementation of this algorithm is done in three stages since determination of velocities requires both accelerations at current and next time step. Firstly, the positions at the next time step are calculated using current velocities and accelerations. The velocity at the next half step $t + \frac{1}{2}\delta t$ can then be determined with

$$\nu(t+\frac{1}{2}\delta t) = \nu(t) + \frac{1}{2}\delta t a(t) \tag{12}$$

After this step, the positions are updated by

$$r(t+\delta t) = r(t) + \frac{1}{2}\delta t\nu(t+\frac{1}{2}\delta t) \tag{13}$$

The new forces can now be determined from current positions, yielding $a(t+\delta t)$. Lastly, velocities at the next time step are computed by

$$\nu(t+\delta t) = \nu(t+\frac{1}{2}\delta t) + \frac{1}{2}\delta t a(t+\delta t) \tag{14}$$

2.3 Monte Carlo

To explain the Monte Carlo (MC) method, which lies at the heart of rare event sampling methods described in this thesis, we start by introducing the classical expression of the partition function Q:

$$Q = c\int dp^N dr^N exp[-H(r^N, p^N)/k_B T] \tag{15}$$

Where r^N stands for the coordinates of all N particles and p^N for their momenta. The function $H(r^N, p^N)$ is the Hamiltonian of the system, a function expressing the total energy of the isolated system as a function of the coordinates and momenta of the particles. Simplified, we can say that $H = K + U$ where K is the kinetic energy of the system and U is the potential energy [30]. c is a constant of proportionality which is chosen so that the sum over quantum states in the calculation of the Helmholtz energy approaches the classical partition function in the limit that $\hbar \to 0$. The

partition function Q itself is central to the sampling of states in a given system since it gives an indication of the number of quantum states that are thermally accessible to the system dependent on the temperature [50]. The classical equation using 15 to obtain the thermal average of an observable A is:

$$\langle A \rangle = \frac{\int dp^N dr^N A(p^N, r^N) exp[-\beta H(p^N, r^N)]}{\int dp^N dr^N exp[-\beta H(p^N, r^N)]} \tag{16}$$

Where $\beta = 1/k_B T$ [30]. The factor $exp[-\beta H(p^N, r^N)]$ is the Boltzmann factor. When a configuration yields high energy the Boltzmann factor naturally goes to zero. The Boltzmann factor is a measure of the probability of any given state. Now we have expressed the variable A as a function of the coordinates and momenta of the constituent particles. The kinetic energy of the system is a quadratic function of the momenta and the integration over momenta can be carried out analytically [30]. The problem here lies not with the momenta, but with the computation of averages that depend on positions, $A(r^N)$. This does not implicate that computing averages that depend on positions are more difficult than averages that depend on both positions and momenta. This is because for most applications, such functions cannot be evaluated analytically, and thus we need numerical solutions to the problem. In most cases, this means we would evaluate (17) by dividing the integrand into a fine mesh of points in the 3N-dimensional configuration space. The total number of points that where the integrand must be evaluated is then equal to m^{3N}. For most systems of interest, this number can become enormous, and just for m=5 and N=100 we would have to evaluate the integrand at 10^{210} points. Even if we could compute this number at a reasonable time, numerical quadrature is a method that works best for smooth functions, but for most intermolecular potentials, the Boltzmann factor in (17) is zero. For example, a liquid of 100 hard spheres at their freezing point would yield a non-zero Boltzmann factor for 1 of 10^{260} configurations [30]. This reveals the need of a better method to compute thermal averages, which we will introduce here as the Monte Carlo importance sampling algorithm [2].

2.3.1 Importance Sampling

If we were to run a brute force MC algorithm, we could determine an integral by evaluating the integrand at a large number of points distributed over the interval of interest. As the number of points approach infinity, we would get an accurate estimate of the integral. However, this would be computationally expensive since the algorithm has to evaluate an infinite number of points, and many of these points are unnecessary to evaluate because they have a negligible Boltzmann factor. Therefore, it would be orders of magnitude more efficient to evaluate such an integral at points where the Boltzmann factor is large and focus less on other regions. This idea is the cornerstone of importance sampling [30]. If we want to sample a one-dimensional integral according to a non-negative probability density, then multiplication of the integral with the probability density would yield areas of importance (where the probability density is high) and areas of little to no importance (where the probability density is close to or at zero). However, since in MC the observables we compute are often averages then many areas of the integral that are equal to zero will greatly influence the average. This however is not an issue since when computing the averages we are often interested in the ratio of two integrals as we will explore with the Metropolis method.

2.3.2 The Metropolis method

Brute force MC is not applicable to evaluating integrals such as $\int dr^N exp[-\beta U(r^N)]$. Fortunately, we are not often interested in the configurational part of the partition function, but rather in averages of observables such as:

$$\langle A \rangle = \frac{\int dr^N exp[-\beta U(r^N)] A(r^N)}{\int dr^N exp[-\beta U(r^N)]} \tag{17}$$

We rather wish to know the ratio of these two integrals [30]. The Metropolis method developed by Metropolis et al. [2] is an effective MC scheme which samples such a ratio. The configurational part of the partition function Z is defined as:

$$Z \equiv \int dr^N exp[-\beta U(r^N)] \tag{18}$$

The ratio $exp-(\beta U)/Z$ in (17) is thus the probability density to find the system in a configuration around r^N [30]. This probability density is known as $N(r^N)$, which is non-negative. If we were to randomly generate points in configuration space by utilising $N(r^N)$, then on average the number of points n_i per unit volume around a point r^N is equal to $LN(r^N)$ where L is the total number of generated points[30]. This means that the observable we wish to compute can be written as:

$$\langle A \rangle \approx \frac{1}{L} \sum_{i=1}^{L} n_i A(r_i^N) \tag{19}$$

As long as we can compute $exp[-\beta U(r^N)]$ then we know the relative probability of visiting different points in space, which again is the cornerstone of the method of importance sampling. Now we must grapple with how to generate points in configuration space according to this relative probability. The usual approach is firstly to prepare the system in a configuration $r^{N(o)}$, denoted by o for old, which must have a non-vanishing Boltzmann factor. Note that the initial configuration does not have to have a high relative probability according to a Boltzmann distribution, as the importance sampling will, given sufficient time, sample this distribution correctly [28]. Now, we can generate a trial configuration, denoted by n for new, by adding a small random displacement Δ to o. The next step is deciding whether to accept or reject the trial configuration. To determine that, we need the Metropolis scheme that determines the transition probability $\pi(o \to n)$ to go from the old configuration to the new one. In any MC simulation where the number of points are larger than the number of accessible configurations, we wish that the number of points at a given configuration is proportional to the probability density at that point. The matrix elements $\pi(o \to n)$ therefore must satisfy the condition that they preserve this equilibrium distribution once it has been reached [30]. For convenience, we apply the condition that in equilibrium, the average number of accepted moves from $o \to n$ is exactly canceled by the number of reverse moves. This condition is known as detailed balance and implies the following:

$$N(o)\pi(o \to n) = N(n)\pi(n \to o) \tag{20}$$

To construct $\pi(o \to n)$ in practice, we need to look at a single MC move. First there is the trial move which changes the configuration of the system. The transition matrix that determines the probability to perform a trial move from $i \to j$ by $\alpha(o \to n)$, where α is the underlying matrix of the Markov chain [8]. Now we must decide by which criteria we accept or reject the trial move. We denote the probability to accept a trial move from $o \to n$ as $acc(o \to n)$. Then:

$$\pi(o \to n) = \alpha(o \to n) \times acc(o \to n) \tag{21}$$

If α is a symmetric matrix then we can rewrite (20) as:

$$N(o) \times acc(o \to n) = N(n) \times acc(n \to o) \tag{22}$$

This means that:

$$\frac{acc(o \to n)}{acc(n \to o)} = \frac{N(n)}{N(o)} = exp\{-\beta[U(n) - U(o)]\} \tag{23}$$

Many possible choices for $acc(o \to n)$ exists, but the choice of Metropolis et al. [2] is:

$$acc(o \to n) = \begin{cases} N(o)/N(n) & \text{if } N(n) < N(o) \\ 1 & \text{if } N(n) \geq N(o) \end{cases} \tag{24}$$

When simulating from less probable statistical configurations, the trial move is always accepted. This also means that configurations which are less likely, but still has a non-zero Boltzmann factor, will get accepted proportional to their statistical weight. This choice of acceptance criterion appears to result in a more efficient sampling of configuration space than most other strategies that have been proposed [30]. To summarise, the transition probability from an old state to a new state is:

$$\pi(o \to n) = \begin{cases} \alpha(o \to n) & N(n) \geq N(o) \\ \alpha(o \to n)[N(n)/N(o)] & N(n) < N(o) \end{cases} \tag{25}$$

$$\pi(o \to o) = 1 - \sum_{n \neq o} \pi(o \to n) \tag{26}$$

The $\pi(o \to o)$ is the rejection probability that recounts the old path. In this summary, α is still undefined which means there is great freedom in fine tuning the trial moves to fit the specifics of the system [30]. The usual procedure of accepting or rejecting a trial move is as follows. If the ratio $N(n)/N(o) > 1$ we immediately accept, and if $N(n)/N(o) < 1$ we generate a random number uniformly between [0-1] and accept the trial move if the random number is smaller than $N(n)/N(o)$. This ensures that, as long as the random number production is truly uniform, the acceptance probability is equal to $N(n)/N(o)$.

2.4 Path Sampling

2.4.1 Transition State Theory

One of the major problems when modelling rare events is the disparity in timescales discussed in section 2.1. Transition State Theory (TST) can be invoked to solve this problem by utilising the dynamical bottleneck for the rare event, also known as the transition state surface[7]. This surface separates the initial and final state of the rare event, such as the reactant and product state of a chemical reaction or two different lattice structures of a crystal. If its location is known, we can construct a scheme where the system is first moved reversibly to the TS surface before releasing many fleeting trajectories from the TS surface. The variable that captures the relevant degrees of freedom for the reaction is known as the reaction coordinate (RC). Along the reaction path, the RC is defined as the negative or positive distance from the point on the reaction path to the saddle point configuration[15] as is typical for low dimensional systems. For systems of higher dimensions, this definition of the RC is not sufficient since the system can transition through several different routes, and thus the RC needs a more robust, complex definition. How this RC should be defined is a topic of ongoing discussion, the points of view being briefly discussed in section 2.4.2.

Step one determines the probability of reaching the transition state whilst step two determines the probability of successfully crossing the threshold. Together, these two steps yield the rate for the rare event [29]. While simple and effective, the major difficulty with this approach is that for complex, high-dimensional systems, identifying the TS surface can be near impossible. Consider figure 3. Here, there is only one truly dynamical way reactive trajectories will traverse to connect the two states, straight through the saddle point. We can easily distinguish in this case that the TS dividing surface should be placed in the xz-plane through the saddle point so that the crossing trajectories are orthogonal to the surface. The issue here is that for most systems of interest, the free energy landscape will rarely resemble this, but rather have a structure such as figure 4. In this free energy landscape there exists a myriad of saddle points situated between the stable states, making it hard to determine which of these are actually important to the rare event. Explicit enumeration of saddle points is feasible for systems consisting of 10 or fewer atoms, but this

provides no means to distinguish between dynamically relevant and irrelevant saddle points[29]. Thus, instead of focusing on an RC that effectively captures the transition, we want to distinguish states through variables known as order parameters (OP).

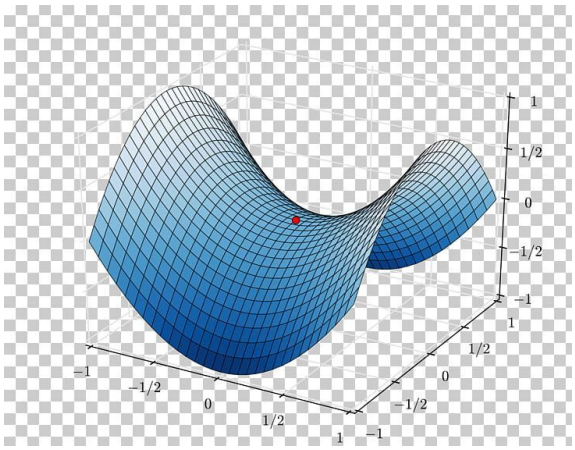

Figure 3: Potential energy landscape of a theoretical low-dimensional rare event where the stable states reside at (0, -1, -1) and (0, 1, -1). The path of lowest energy connecting the states passes straight through the saddle point (the red dot), which resides at the transition state. Picture from [53].

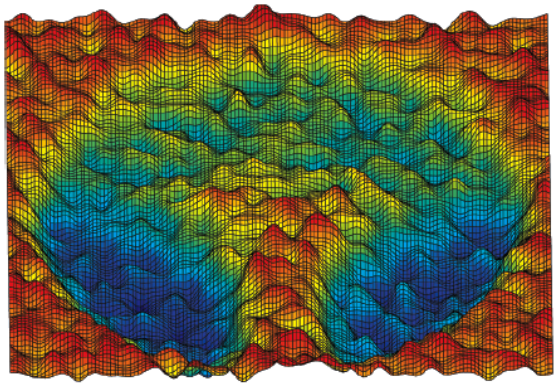

Figure 4: Potential energy landscape of a theoretical high-dimensional rare event. The stable states here reside in the dark blue valleys. There are a number of potential saddle points between these regions, but most of them will likely not be dynamical. Picture from [54].

2.4.2 Order Parameters & Reaction Coordinates

Most advanced methods of sampling rare event trajectories distinguish the states by introducing OPs. TPS mainly relies on using OPs to distinguish between states as opposed to using RCs. However, depending on the application and user, these two concepts might be regarded interchangeably and the definitions are not so clear. If TPS is mainly a method that seeks to only generate transition paths then we do not need a RC. However, if a reaction rate determination is being done through TPS, then the need for only an OP is questionable[48]. Some claim that there should be only one, ultimate RC which is the committor function which defines for every phase point a probability that a trajectory starting from that point ends in B rather than A. Other times, the parameter chosen for the importance sampling is known as the RC and the OP is any other parameter used in post analysis[48]. An OP q is usually low-dimensional, utilising the degrees of freedom best suited for separating the initial and final regions. These regions must be characterised carefully and is by no means trivial, since poor definitions will lead to erroneous results. There are several criteria which must be satisfied for the OP to operate efficiently. First, both regions A and B must be sufficiently large as to accommodate equilibrium fluctuations in their respective

basins of attraction [33]. A basin of attraction is defined as a region in configuration space where trajectories are likely to relax into the basins corresponding stable state. If this criterion is not met then the sampling will give rise to undynamical transition pathways. This means that region A should never overlap with region B's basin of attraction and vice versa [33]. This problem is shown in figure 5. Fortunately, it is easy to figure out if an order parameter is wrong, since uncharacteristically short trajectories will begin from A and end in B with a probability near 1 due to part of A being located in the basin of attraction of B.

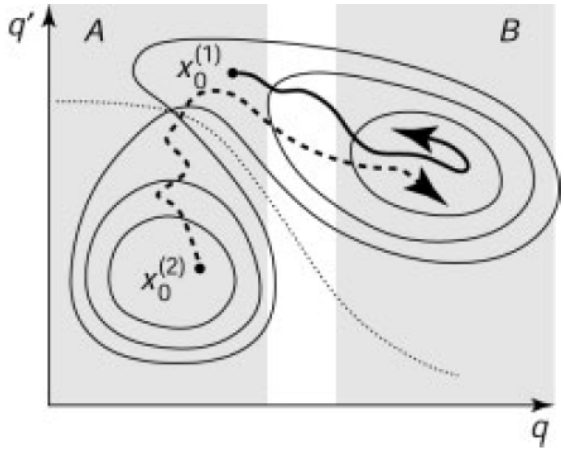

Figure 5: Free energy landscape along two degrees of freedom q and q'. The grey area represents the proposed stable states along q with the solid lines indicating the basins of attraction of each state. Both trajectories start from stable state A and end in B, however the first path (solid line from $x_0^{(1)}$) is located within B's basin of attraction and will almost always relax into B, meaning that this is not a true transition path. The second path (dashed line from $x_0^{(2)}$) is a transition path as it starts in A's basin of attraction before crossing to B. The small dashed line which bisects the two basins of attraction is where the ideal separation of states should be, indicating that we must account for the effect of q' as well. Figure from [33].

2.4.3 Transition Path Ensemble

In order to successfully sample a collection of the statistical dynamical pathways connecting states A and B, we must first define the Transition Path Ensemble (TPE). If the system is ergodic, meaning that every point in phase space has a non-zero probability to be visited [26], then every possible reactive dynamical trajectory will occur with a certain probability. This can be used to construct a distribution functional for dynamical trajectories upon which we base the statistical mechanics of the trajectories [33]. With such a functional, one can derive partition functions for ensembles of trajectories which satisfy desired constraints which is at the core of the TPS method [33, 38, 42]. We denote a trajectory of length T by $x(T)$ where we have discretised the time evolution so that we can represent the trajectory as an ordered sequence of states from start to finish, $x(T) \equiv \{x_0, x_{\Delta t}, x_{2\Delta t}, ..., x_T\}$. Each state, known as time slices, are separated by small time increments Δt. Each time slice contains all the variables needed to describe the system at that point in phase space. The statistical weight, $P[x(T)]$ of any trajectory depends on the distribution of initial conditions and on the specific propagation rules describing the time evolution of the system [33]. If, for example, we have a Markovian system where state x_t goes to $x_{t+\Delta t}$ with probability $p(x_t \to x_{t+\Delta t})$, we can express the dynamical path probability as a product of short-time transition probabilities [33]:

$$P[x(T)] = \rho(x_0) \prod_{i=0}^{T/\Delta t - 1} p(x_{i\Delta t} \to x_{(i+1)\Delta t}) \tag{27}$$

$\rho(x_0)$ is here the distribution of states x_0 which are the starting points for the trajectories. We

can expand upon this definition by adding the restriction that only reactive trajectories need be considered, the trajectories that begin in region A at time zero and ending in region B at time T.

$$P_{AB}[x(T)] \equiv h_A(x_0)P[x(T)]h_B(x_T)/Z_{AB}(T) \tag{28}$$

$h_A(x)$ and $h_B(x)$ are the population functions which are equal to 1 if the path starts in A and ends in B, and is zero otherwise. Z_{AB} is a factor which normalises the distribution of trajectories:

$$Z_{AB}(T) \equiv \int dx(T)h_A(x_0)P[x(T)]h_B(x_T) \tag{29}$$

The notation $dx(T)$ indicates that we sum over all trajectories $x(T)$ and since we have a discretisation of paths this corresponds to integration over states at each time slice [33].

2.4.4 Deterministic Dynamics

When using deterministic dynamics, the time evolution of the system is solely determined by the initial conditions [33]. The system is here described by a set of differential equations

$$\dot{x} = \Gamma(x) \tag{30}$$

where $\dot{x}$ is the time derivative of x and $\Gamma(x)$ is a function dependent only on x. Newtonian motion is described in this way, with position and momenta being represented as

$$\dot{r} = \frac{\delta H(r,p)}{\delta p} \tag{31}$$

$$\dot{p} = -\frac{\delta H(r,p)}{\delta r} \tag{32}$$

Other than Newtonian dynamics there are equations of motion derived from the Lagrangian of Car and Parrinello[11], for various thermostatted systems [14] and several other types of dynamics. After solving (30) we get the propagator ϕ_t [33] which links the initial state to the state at time t

$$x_t = \phi_t(x_0) \tag{33}$$

This clearly shows that x_t will evolve into $x_{t+\Delta t}$ given a time change Δt. The short time transition probability is given by a Dirac delta function [33]

$$p(x_t \to x_{t+\Delta t}) = \delta[x_{t+\Delta t} - \phi_{\Delta t}(x_t)] \tag{34}$$

This delta function takes an argument of a high-dimensional vector containing all positions and momenta necessary to describe a Newtonian system. We can partition this delta function into a product of delta functions each representing a single coordinate. Thus, the reactive path probability for a deterministic trajectory is

$$P_{AB}[x(T)] = \rho(x_0)h_A(x_0)\left\{\prod_{i=0}^{T/\Delta t-1} \delta[x_{(i+1)\Delta t} - \phi_{\Delta t}(x_{i\Delta t})]\right\} h_B(x_T)/Z_{AB}(T) \tag{35}$$

The normalisation factor $Z_{AB}(T)$ is given by

$$Z_{AB}(T) = \int dx_0 \rho(x_0) h_A(x_0) h_B(x_T) \tag{36}$$

Integration have here been carried out over all states along the trajectory except for at time zero.

2.4.5 Stochastic Dynamics

Analysing the studied system can often be simplified by replacing some degrees of freedom with random noise[33]. This makes it so that the other degrees of freedom x can be described by a Langevin equation. If the random noise is uncorrelated in time we get

$$\dot{r} = \frac{p}{m} \tag{37}$$

$$\dot{p} = F(r) + \gamma p + R \tag{38}$$

$F(r)$ is the force dependent on the potential energy $V(r)$, γ is the friction constant and R is the random force which is related by the fluctuation dissipation theorem

$$\langle R(t)R(0)\rangle = 2m\gamma k_B T\delta(t) \tag{39}$$

Where T us the temperature and k_B is the Boltzmann constant. The random noise R compensates for the energy lost by the friction $-\gamma p$. Several algorithm exist to solve (38) over the time increments Δt [12]. These algorithms, which provide stochastic trajectories through repetition, take the form of

$$x_{t+\delta t} = x_t + \delta x_S + \delta x_R \tag{40}$$

The systematic part δx_S is determined solely by x_t and the random part δx_R is drawn from a distribution $w(\delta x_R)$[33]. In Langevin dynamics, this distribution is a multivariate Gaussian distribution [1]. This random component dampens the time evolution such that several states are accessible from any starting configuration [33]. The single-step transition probability is given by

$$p(x_T \to x_{t+\Delta t}) = w(\delta x_R)|\frac{d\delta x_R}{dx_{t+\Delta t}}| \tag{41}$$

The right hand side is a Jacobian that arises from the variable transformation from random displacement δx_R to the phase space point $x_{t+\Delta t}$[33]. In [12] this Jacobian is unity which simplifies the path weight[23]. This transition probability is also normalised and conserves the canonical distribution as required by (39) [23]. By concatenation of the transition probabilities in (41) and with boundary conditions, the reactive path probability becomes

$$P_{AB}[x(T)] = \rho(x_0)h_A(x_0)\left\{\prod_{i=0}^{T/\Delta t-1} w[x_{(i+1)\Delta t} - x_{i\Delta t} - \delta x_S]\right\} h_B(x_T)/Z_{AB}(T) \tag{42}$$

2.5 Sampling procedure

In order to sample the TP ensemble, we employ techniques for modifying existing reactive trajectories by way of Monte Carlo moves [29, 33, 34, 37, 38, 48]. TPS is an importance sampling based technique as described in section 2.3.1, so we must use a scheme wherein each trajectory is sampled according to its statistical weight from a Boltzmann distribution. To accomplish this, we

start with a reactive path $x^{(o)}(T)$ (o meaning old path), which has a nonzero weight according to a Boltzmann distribution. By modifying the old path we can now generate a new path $x^{(n)}(T)$. If accepted, the new path will become the old path and the process is started anew. In standard MC approaches, this is known as a *trial move*. When discussing trial moves, we need to derive a proper acceptance criterion that obeys Metropolis-Hastings for each specific trial move. The acceptance rate of new paths are dependent on the move, however we are not interested in always attaining a high acceptance rate as this would involve new paths that are very similar to the old ones which leads to slow convergence and strong correlation. In this chapter, we will define the most common TP moves and discuss them, and later we shall derive the proper acceptance criterion for each move.

2.5.1 Detailed Balance

Detailed balance is an acceptance criterion which is simple yet powerful. It states that the frequency of accepted moves from old to new path must be exactly balanced by the frequency of reverse moves [3, 33]. This can be expressed mathematically as

$$P_{AB}[x^{(o)}(T)]\pi[x^{(o)}(T) \to x^{(n)}(T)] = P_{AB}[x^{(n)}(T)]\pi[x^{(n)}(T) \to x^{(o)}(T)] \tag{43}$$

Here, $\pi[x(T) \to x'(T)]$ is the conditional probability of going from $x(T)$ to $x'(T)$ given initial path $x(T)$. This means that $\pi[x(T) \to x'(T)]$ is the product of the probability to create $x'(T)$ from $x(T)$, $P_{gen}[x(T) \to x'(T)]$, and the probability to accept the new path $x'(T)$, $P_{acc}[x(T) \to x'(T)]$ [33]. From detailed balance, we get a condition for the acceptance probability

$$\frac{P_{acc}[x^{(o)}(T) \to x^{(n)}(T)]}{P_{acc}[x^{(n)}(T) \to x^{(o)}(T)]} = \frac{P_{AB}[x^{(n)}(T)]P_{gen}[x^{(n)}(T) \to x^{(o)}(T)]}{P_{AB}[x^{(o)}(T)]P_{gen}[x^{(o)}(T) \to x^{(n)}(T)]} \tag{44}$$

This condition is satisfied by applying the Metropolis-Hastings rule since P_{gen} is not symmetric and thus does not cancel out.

$$P_{acc}[x^{(o)}(T) \to x^{(n)}(T)] = min\{1, \frac{P_{AB}[x^{(n)}(T)]P_{gen}[x^{(n)}(T) \to x^{(o)}(T)]}{P_{AB}[x^{(o)}(T)]P_{gen}[x^{(o)}(T) \to x^{(n)}(T)]}\} \tag{45}$$

For simplicity we use the indicator functions $h_A(0)$ and $h_B(T)$ to express the acceptance probability as

$$P_{acc}[x^{(o)}(T) \to x^{(n)}(T)] = h_A[x_0^{(n)}]h_B[x_T^{(n)}] \times min\left\{1, \frac{P[x^{(n)}(T)]P_{gen}[x^{(n)}(T) \to x^{(o)}(T)]}{P[x^{(o)}(T)]P_{gen}[x^{(o)}(T) \to x^{(n)}(T)]}\right\} \tag{46}$$

where $x_0^{(n)}$ and $x_T^{(n)}$ are the first and last state of the trial trajectory, respectively.

2.5.2 Shooting moves

So far, the most common move in TPS and all techniques derived from it is the shooting move. Here, a phase-space point is selected from the old reactive pathway and is modified to yield new initial conditions. After the phase-space point is modified, we then generate a new trajectory by generating the path forwards and backwards in time until the path extends from $t = 0$ to $t = T$ [33]. The generation of a new path is based on the dynamics of the system at hand, starting from the shooting point t' and ending in T for forwards generation, and 0 for backwards, the generation probabilities become

$$P^f_{gen}[o \to n] = \prod_{i=t'/\Delta t}^{T/\Delta t-1} p[x^{(n)}_{i\Delta t} \to x^{(n)}_{(i+1)\Delta t}] \tag{47}$$

$$P^b_{gen}[o \to n] = \prod_{i=1}^{t'/\Delta t} \bar{p}[x^{(n)}_{i\Delta t} \to x^{(n)}_{(i-1)\Delta t}] \tag{48}$$

With $\bar{p}(x \to x) = p(\bar{x} \to \bar{x})$ with $\bar{x} = \{r, -p\}$. By combining both the forward and backward generation probabilities with the probability of generating the new phase space shooting point from the old point, we get the complete generation probability for the path [33].

$$P_{gen}[x^{(o)}(T) \to x^{(n)}(T)] = p_{gen}[x^{(o)}_{t'} \to x^{(n)}_{t'}] \prod_{i=t'/\Delta t}^{T/\Delta t-1} p[x^{(n)}_{i\Delta t} \to x^{(n)}_{(i+1)\Delta t}] \times \prod_{i=1}^{t'/\Delta t} \bar{p}[x^{(n)}_{i\Delta t} \to x^{(n)}_{(i-1)\Delta t}] \tag{49}$$

This generation probability can be used to determine the acceptance probability of a shooting move by way of (46). For this purpose, we express the ratio in the second argument through dynamical path probability, as a product of short-time transition probabilities

$$P[x(T)] = \rho(x_0) \prod_{i=0}^{T/\Delta t-1} p(x_{i\Delta t} \to x_{(i+1)\Delta t}) \tag{50}$$

Where $\rho(x_0)$ is the distribution of states x_0 which are the starting points for $x(T)$. Together with (49), we find

$$\frac{P[x^{(n)}(T)]P_{gen}[x^{(n)}(T) \to x^{(o)}(T)]}{P[x^{(o)}(T)]P_{gen}[x^{(o)}(T) \to x^{(n)}(T)]} = \frac{\rho[x^{(n)}_0]p_{gen}[x^{(n)}_{t'} \to x^{(o)}_{t'}]}{\rho[x^{(o)}_0]p_{gen}[x^{(o)}_{t'} \to x^{(n)}_{t'}]} \prod_{i=0}^{t'/\Delta t-1} \frac{p[x^{(n)}_{i\Delta t} \to x^{(n)}_{(i+1)\Delta t}]}{\bar{p}[x^{(n)}_{(i+1)\Delta t} \to x^{(n)}_{i\Delta t}]} \times \frac{\bar{p}[x^{(o)}_{(i+1)\Delta t} \to x^{(o)}_{i\Delta t}]}{p[x^{(o)}_{i\Delta t} \to x^{(o)}_{(i+1)\Delta t}]} \tag{51}$$

This result can be simplified if the dynamics conserve a stationary distribution $\rho_{st}(x)$, which is a general condition applying to systems at equilibrium among others[33]. In fact, detailed balance only holds at equilibrium, and non-equilibrium steady states has to be maintained by cyclic processes [3]. Regardless, we find that p and $\bar{p}$ are related through microscopic reversibility

$$\frac{p(x \to y)}{\bar{p}(y \to x)} = \frac{\rho_{st}(y)}{\rho_{st}(x)} \tag{52}$$

By using this in (51) and utilising (46), we get an acceptance probability

$$P_{acc}[x^{(o)}(T) \to x^{(n)}(T)] = h_A[x^{(n)}_0]h_B[x^{(n)}_T] \times min\{1, \frac{\rho[x^{(n)}_0]}{\rho[x^{(o)}_0]} \frac{\rho_{st}[x^{(o)}_0]}{\rho_{st}[x^{(n)}_0]} \frac{\rho_{st}[x^{(n)}_{t'}]}{\rho_{st}[x^{(o)}_{t'}]} \frac{p_{gen}[x^{(n)}_{t'} \to x^{(o)}_{t'}]}{p_{gen}[x^{(o)}_{t'} \to x^{(n)}_{t'}]}\} \tag{53}$$

However, the distribution of initial conditions is usually an equilibrium distribution and thus identical to the conserved distribution, simplifying the acceptance probability even more [33]

$$P_{acc}[x^{(o)}(T) \to x^{(n)}(T)] = h_A[x^{(n)}_0]h_B[x^{(n)}_T] \times min\{1, \frac{\rho_{st}[x^{(n)}_{t'}]}{\rho_{st}[x^{(o)}_{t'}]} \times \frac{p_{gen}[x^{(n)}_{t'} \to x^{(o)}_{t'}]}{p_{gen}[x^{(o)}_{t'} \to x^{(n)}_{t'}]}\} \tag{54}$$

In most cases, the modification of the shooting point is symmetric such that the last ratio also cancels so that

$$P_{acc}[x^{(o)}(T) \to x^{(n)}(T)] = h_A[x_0^{(n)}]h_B[x_T^{(n)}] \times min\{1, \frac{\rho_{st}[x_{t'}^{(n)}]}{\rho_{st}[x_{t'}^{(o)}]}\} \tag{55}$$

2.5.3 Deterministic considerations

Next we discuss how effective shooting moves can be implemented for deterministic systems. Since the trajectory is ultimately determined by the initial conditions, picking a point t' along an old trajectory and propagating forwards and backwards will always yield the exact same path. Therefore, the shooting point must be modified in some way. This modification is usually in the form of atomistic displacements such as altering the atomic momenta. This is usually accomplished by drawing a perturbation δp from a Gaussian distribution with a mean of zero and a variance set by the user. The advantage of using a Gaussian distribution is that it is symmetric, meaning the generation probability of going from $x_{t'}^{(o)} \to x_{t'}^{(n)}$ is identical to its reverse, preserving detailed balance. Caution must be taken when determining the magnitude of displacement. If the displacement is too large, we might end up generating a lot of undynamical pathways which would not be accepted, and if the displacement is too small we end up with paths that are too similar to the old one. Note that in some instances, changing both configuration and momentum at the shooting point can be advantageous for more efficient sampling [25]. Growing the trajectory after modifying the shooting point is done in two steps. First, the forward segment of the trajectory is grown by integrating for the appropriate number of time steps [33]. The backwards segment has to be grown with inverted direction of time. If the dynamics are time-reversible, we do this by inverting all momenta and integrating forward in time [33], such that $\bar{p}(x \to y) = p(\bar{x} \to \bar{y})$ with $\bar{x} = \{r, -p\}$.

2.5.4 Stochastic Considerations

For most applications, shooting moves for stochastic dynamics are identical to their deterministic counterparts. However there are some important differences. With a reactive stochastic path $x^{(o)}(T)$, we can select a random point $x_{t'}^{(o)}$ and initiate a stochastic trajectory by integrating forward in time. Similarly the backwards segment is grown with time inverted dynamics[33]. The key difference is that you do not need a modification of the shooting point since stochastic elements are not solely determined by the initial conditions. This makes it so that the generation probability is symmetric so the acceptance probability becomes

$$P_{acc}[x^{(o)}(T) \to x^{(n)}(T)] = h_A[x_0^{(n)}]h_B[x_T^{(n)}] \tag{56}$$

Which makes it so that any reactive pathway can be accepted. Time does not appear in the Metropolis MC transition probability so forward and backwards integration are identical, meaning backwards trajectories can be grown with the forward propagation rule [33].

$$\frac{p(x \to y)}{p(y \to x)} = exp\{-\beta[H(y) - H(x)]\} \tag{57}$$

In addition, stochastic trajectories can be grown in a single direction only from the shooting point, and simply replacing the other segment with that of the old one which will yield a path with a nonzero dynamical weight. This is opposed to deterministic dynamics where this would result in a path of zero weight.

2.6 Rate computation

The most fundamental advantage of TPS is that the ensembles produced consist of purely dynamical pathways, free of any bias. This means they can be used to compute dynamical constants, particularly rate constants k_{AB} and k_{BA} for the forwards and backwards reaction, respectively. The calculation of rate constants with this method requires no *a priori* knowledge of reaction mechanism, which gives it an edge over other methods such as the Bennett-Chandler approach [22, 33, 38]. As discussed in section 2.4.1, by invoking transition state theory the rate constant determination is done in two steps, where the choice of RC is vital to the success. In TPS, the method relies on a computed time correlation function as a ratio of partition functions for different ensembles, which may be considered as the exponential of the work to reversibly confine the final state of any trajectory to state B[33]. Since the crossing events of interest are rare, the work is large and cannot be determined directly. Thus, we use other techniques of approximation such as umbrella sampling [44].

2.6.1 Time correlation function

Whilst at equilibrium, populations of state A and B fluctuate because of spontaneous transitions. The dynamics of this is expressed by the correlation of state populations as a function time

$$C(t) \equiv \frac{\langle h_A(x_0) h_B(x_t) \rangle}{\langle h_A(x_0) \rangle} \tag{58}$$

With $\langle ... \rangle$ meaning the average over the equilibrium ensemble of initial conditions [33]. $C(t)$ can be understood as the conditional probability to find the system in state B at time t given that it was in state A at time 0. The fluctuation-dissipation theorem (39) [13] states that dynamics of equilibrium fluctuations are equivalent to the relaxation from a nonequilibrium state in which only state A is populated. At long timescales, these nonequilibrium dynamics are described the phenomenology of macroscopic kinetics. This means that the behaviour of *C(t)* is determined by k_{AB} and k_{BA}. Given sufficient time, and provided there is a single dynamical bottleneck separating the states, the time correlation function can be expressed as

$$C(t) \approx \langle h_B \rangle (1 - exp\{-t/\tau_{rxn}\}) \tag{59}$$

Given a short time regime, *C(t)* reflects microscopic motions in the TS region correlated over the timescale τ_{mol}, which is the minimum time required to cross the dynamical bottleneck and commit to a stable state. (59) connects the reaction time τ_{rxn} which can be measured experimentally, with the microscopic correlation function *C(t)* [33]. For longer times we expect, given that the transition kinetics are two-state:

$$C(t) \approx k_{AB} t \tag{60}$$

The slope of *C(t)* in this region is equal to k_{AB}. As long as we can determine *C(t)* for times larger than τ_{mol} we can extract rate constants from *C(t)*. In terms of TPS, we can write *C(t)* as sums over trajectories

$$C(t) = \frac{\int Dx(t) h_A(x_0) P[x(t)] h_B(x_t)}{\int Dx(t) h_A(x_0) P[x(t)]} = \frac{Z_{AB}(t)}{Z_A} \tag{61}$$

$Z_{AB}(t)$ is the partition function for the ensemble that begins in A and ends in B at time t. Z_A is the partition function for the ensemble of every trajectory that starts in A and ends anywhere at t, including B. This implies that $Z_A \geq Z_{AB}(t)$. Z_A has no time argument since the dynamical weight is normalised, meaning Z_A is the equilibrium probability of finding the system in A. We can

interpret this ratio of partition functions as the exponential of a reversible work $W_{AB}(t)$ necessary to change between the ensembles [33].

$$W_{AB} \equiv -ln\frac{Z_{AB}(t)}{Z_A} \tag{62}$$

W_{AB} corresponds to a shift in free energy needed to confine all trajectory endpoints x_t to B while still maintaining that all initial points x_0 is in A.

2.6.2 Umbrella Sampling

To overcome a free energy barrier which is large compared to k_BT, we introduce an artificial bias potential, $U(x)$[22, 24, 30]. In a simple case, we set $U(x)$ so that the importance sampling scheme visits rare but dynamically interesting states as often as equilibrium states. This makes it so that free energy differences can be directly calculated after correcting for the presence of $U(x)$. If phase space is large however, it is advantageous to divide space into several overlapping "windows" [22]. Here, the ith bias restrains the system to the ith window. This overlapping series of windows can now be put at the dynamical bottleneck between A and B and $U(x)$ can be applied such that whenever a trial move is attempted, $U(x)$ adds a potential energy which is infinite outside the ith window and zero within it. With a good choice of the window boundaries $\lambda^{(i)}$, the distribution of λ, $P(\lambda)$ will not vary considerably within each window [33]. Within a window, $P(\lambda)$ can be calculated up to a constant of proportionality with importance sampling. w_B can then be computed by integrating over the OP distribution

$$w_B = -k_BT \cdot ln \int_{\lambda^B_{min}}^{\lambda^B_{max}} d\lambda P(\lambda) \tag{63}$$

This describes a more general approach, and we extend it to ensembles of trajectories by focusing on calculating the reversible work needed to restrain trajectories endpoints to B given that they start in A. That means we need to compute $P_A(\lambda, t)$, the distribution of λ at the endpoints of trajectories that starts in A. Within every window, this distribution can also be calculated up to a constant of proportionality with TPS. The distribution of paths that start in A and ends in the window region $W[i]$, $P_{AW[i]}(\lambda, t)$, is proportional to the complete OP distribution $P_A(\lambda, t)$ which can be obtained as an average over pathways with unrestricted endpoints. The reversible work required to confine the endpoints of paths from A to B is

$$W_{AB}(t) = -ln \int_{\lambda^B_{min}}^{\lambda^B_{max}} d\lambda P_A(\lambda, t) \tag{64}$$

2.7 Transition Interface Sampling

Transition Interface Sampling (TIS) uses the mathematical framework of TPS, but instead of needing paths to cross from state A to B directly, a set of hypersurfaces known as interfaces are introduced in phase space that separate A and B. This method provides some advantages over TPS, such as allowing for variable path length and being less sensitive to recrossings [37]. TIS as a method measures the effective positive flux through these interfaces, as opposed to the general conditional flux of TPS as in (58). In order to achieve a framework where this is possible, we define *overall states* **A** and **B**. We first consider a set of $n+1$ non-intersecting interfaces which are described by our OP $\lambda(x)$. Next, we set $\lambda_i, i = 0, ..., n$ so $\lambda_{i-1} < \lambda_i$ and the boundaries of A and B are defined by λ_0 and λ_n, respectively. For every point in phase space x and every interface i, we define a backwards time $t_i^b(x)$ and forwards time $t_i^f(x)$[37]

$$t_i^b(x_0) \equiv -max[\{t|\lambda(x_t) = \lambda_i \wedge t \leq 0\}] \tag{65}$$
$$t_i^f(x_0) \equiv +min[\{t|\lambda(x_t) = \lambda_i \wedge t \geq 0\}] \tag{66}$$

These times marks the points of first crossing with interface i from a trajectory starting in x_0. Next, we introduce two-fold characteristic functions that depend on two interfaces $i \neq j$

$$h_{i,j}^b(x) = \begin{cases} 1 & \text{if } t_i^b(x) < t_j^b(x), \\ 0 & \text{otherwise} \end{cases} \tag{67}$$
$$h_{i,j}^f(x) = \begin{cases} 1 & \text{if } t_i^f(x) < t_j^f(x), \\ 0 & \text{otherwise} \end{cases} \tag{68}$$

These functions determine whether the respective time evolution of the trajectory will reach interface i before j. Since the interfaces does not intersect, time evolution need only be evaluated for phase points x that are between i and j, and if the system is ergodic then both interfaces will be crossed in a finite amount of time, making it so $h_{i,j}^b(x) + h_{j,i}^b(x) = h_{i,j}^f(x) + h_{j,i}^f(x) = 1$. Both backward characteristic functions define the *overall states* **A** and **B**

$$h_{\mathbf{A}}(x) = h_{0,n}^b(x) \tag{69}$$
$$h_{\mathbf{B}}(x) = h_{n,0}^b(x) \tag{70}$$

Overall states **A** and **B** span the complete phase space. Effectively, a trajectory is counted as being part of an overall state if the trajectory is either currently residing in that state, or has most recently visited that state. This is schematically depicted in figure 6. This means that the overall states does not depend heavily on the stable state definition. The advantage of using overall states is that they limit the sensitivity that TPS has on recrossings into the same stable state a trajectory was initiated from. With this definition, we can now express the rate equation, with $\dot{h}_B$ meaning the time derivative taken at $t = 0$, as

$$k_{AB} = \frac{\langle h_A(x_0)\dot{h}_B(x_0)\rangle}{\langle h_A(x_0)\rangle} \tag{71}$$

The rate expression in (71) is independent of time, even though evaluating the characteristic functions requires integration of motion [34]. Figure 6 shows that a transition from **A** into **B** will only count the first crossing with λ_B and every subsequent crossing into **B** will not be counted unless the system has returned to **A** again. Our OP should be sufficiently defined so that this probability of $\mathbf{B} \to \mathbf{A}$ is equal to $\mathbf{A} \to \mathbf{B}$, meaning every recrossing to the other overall state is a new rare event. This scheme makes it so that (71) is equal to the effective positive flux expression [34]

$$k_{AB} = \frac{\langle h_A(x_0)\lambda(x_0)\theta(\lambda(x_0))\delta(\lambda(x_0) - \lambda_B)\rangle}{\langle h_A(x_0)\rangle} \tag{72}$$
$$= \lim_{\Delta t \to 0} \frac{1}{\Delta t} \frac{\langle h_A(x_0)\theta(\lambda_B - \lambda(x_0))\theta(\lambda(x_{\Delta t}) - \lambda_B)\rangle}{\langle h_A(x_0)\rangle} \tag{73}$$

The last expression here is the most applicable for a numerical approach with Δt as the time step in an MD simulation [34]. Evaluating (72) requires a counting of all phase space points which at $t = 0$ are close to crossing λ_B in a single time step and will enter **A** before **B** when integrating

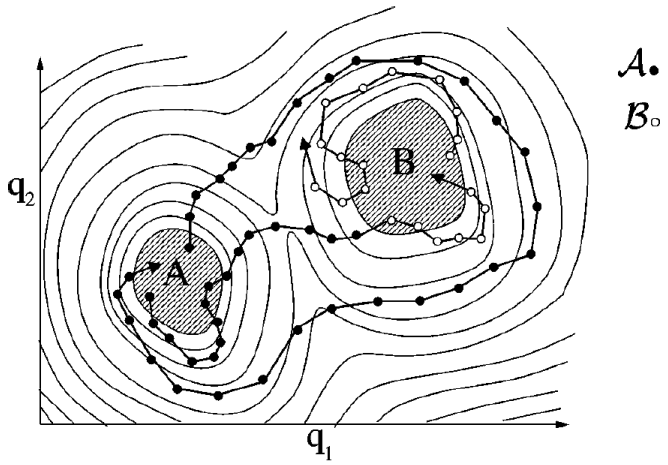

Figure 6: Two-dimensional free energy profile along two OPs q_1 and q_2. The thin solid lines represent the free energy contour lines. The solid dotted black lines represent trajectories, with the arrow indicating the endpoint and the dots representing each successive time step. A dot is coloured black if the trajectory at that time step is part of **A** and white if it is part **B**. Picture from [34].

backwards in time from x_0. This however is not efficient computationally since only a few points close to λ_B belongs to **A**. This can be improved upon by relating the flux through λ_B to the flux through interfaces between the stable states. To achieve this, we use the set of n non-intersecting interfaces with λ_i being closer to stable state A than λ_{i+1}. Next, we need to introduce some crossing probabilities depending on four non-intersecting interfaces $\{x|\lambda(x) = \lambda_i\}$, $\{x|\lambda(x) = \lambda_j\}$, $\{x|\lambda(x) = \lambda_k\}$ and $\{x|\lambda(x) = \lambda_l\}$

$$P(^{k}_{l}|^{j}_{i}) = \lim_{dt\to 0} \frac{\langle h^b_{ij}(x_0)\theta(\lambda_j - \lambda(x_0))\theta(\lambda(x_{dt}) - \lambda_j)h^f_{kl}(x_0)\rangle}{\langle h^b_{ij}(x_0)\theta(\lambda_j - \lambda(x_0))\theta(\lambda(x_{dt}) - \lambda_j)\rangle} \tag{74}$$

$$= \frac{h^b_{ij}(x_0)\dot{\lambda}(x_0)\delta(\lambda(x_0) - \lambda_j)\theta(\dot{\lambda}(x_0))h^f_{kl}(x_0)\rangle}{\langle h^b_{ij}(x_0)\dot{\lambda}(x_0)\delta(\lambda(x_0) - \lambda_j)\theta(\dot{\lambda}(x_0))\rangle} \text{ for } \lambda_j > \lambda_i \tag{75}$$

..

This equation defines a conditional crossing probability under the conditions that the system should cross λ_j at time $t = 0$ and that λ_i has been more recently crossed than λ_j[46]. With these crossing probabilities, (72) is equal to the product of the initial flux and the overall crossing probability [34].

$$k_{AB} = \frac{\langle\dot{\lambda}(x_0)\delta(\lambda(x_0) - \lambda_0)\theta(\dot{\lambda}(x_0))\rangle}{\langle h_A(x_0)\rangle} \times P(^{n}_{0}|^{0}_{0^-}) \equiv f_A P_A(\lambda_n|\lambda_0) \tag{76}$$

f_A is the flux inside A which is computed with an MD run. 0^- is to denote an interface $\lambda_0 - \epsilon$ to indicate the direction of crossing at $t = 0$ [46]. The total crossing probability $P_A(\lambda_n|\lambda_0)$ can be interpreted as when λ_0 is crossed then λ_n will be crossed before recrossing to λ_0. This probability can be computed with the set of $n - 1$ non-intersecting interfaces such that the overall crossing probability can be defined as[34]

$$P_A(\lambda_n|\lambda_0) = \prod_{i=0}^{n-1} P_A(\lambda_{i+1}|\lambda_i) \tag{77}$$

This expression is central to TIS. In this equation, we can determine a continuous crossing probability function for any λ between λ_1 and λ_B. If the overall crossing probability from stable state

A to B in a rare event is 10^{-6} then MD will have to sample a million paths in the $[0^+]$ and $[0^-]$ ensembles[48]. In TIS, we usually want to sample equally between all path ensembles. With 6 interfaces placed so that $P_A(\lambda_{i+1}|\lambda_i) \approx 0.1$, we can get an estimate of the overall crossing probability with a minimum of 10 paths each in the $[0^+]$, $[1^+]$, $[2^+]$, $[3^+]$, $[4^+]$ and $[5^+]$, reducing the minimum amount of paths from one million to 60. In order to measure the effective positive flux f_A, a plain MD simulation can be run to determine

$$f_A = \frac{N_c^+}{T_{\in A}} \tag{78}$$

N_c^+ is the integer of positive crossings with interface λ_0 and $T_{\in A}$ is the time the system spends in **A**. The transition to **B** is often a rare event, so the denominator of (78) will often be equal to 1.

2.8 Replica Exchange Transition Interface Sampling

Replica Exchange TIS (RETIS) is a method that builds upon the TIS algorithm by introducing a swapping scheme. This means that the algorithm can exchange trajectories between the different ensembles. There are two main differences that sets this method apart from TIS, the introduction of the $[0^-]$ ensemble and the swapping move. The $[0^-]$ ensemble is used to both study the stable state A of the system as well as to calculate the effective positive flux. (78) shows how the effective positive flux is calculated by an MD simulation. RETIS on the other hand is exclusively based on path sampling, meaning f_A is also determined this way. To compute f_A, the $[0^-]$ ensemble is introduced which is composed of all paths that starts at λ_0 and progresses away from λ_n, i.e. back into A, before returning to λ_0. This allows us to calculate f_A via the average path lengths $\langle t^{[0^+]} \rangle$ and $\langle t^{[0^-]} \rangle$ of the paths in the $[0^+]$ and $[0^-]$ ensembles, respectively.

$$f_A = \frac{1}{\langle t^{[0^+]} \rangle + \langle t^{[0^-]} \rangle} \tag{79}$$

Next we shall discuss the new moves implemented by RETIS. The first is the time-reversal move. This is a cost-free move which does not require integration as the move entails changing the time direction of a trajectory whilst simultaneously inverting all velocities. The other move is the swapping move (replica exchange) which exchanges paths between ensembles. The swapping between $[i^+] \leftrightarrow [(i+1)^+]$ is accepted if the $[i^+]$ path crosses λ_{i+1}. The special case is $[0^+] \leftrightarrow [0^-]$ swap which is always accepted. In this move, a new $[0^+]$ path is created by taking the endpoint of an existing path in the $[0^-]$ ensemble. The trajectory is then integrated forwards in time from the endpoint until the trajectory reaches λ_A. Similarly, a path in the $[0^-]$ ensemble is created with the start point of an existing path in the $[0^+]$ ensemble, from where the trajectory is grown backwards in time until it reaches λ_A. This move in particular helps the ergodicity of the sampling [48]. The familiar shooting move discussed in section 2.5.2 is also used in RETIS. Overall crossing probabilities provided by RETIS usually gives smoother curves than TIS [41]. A schematic depiction of the various moves employed by RETIS is given in figure 7. With this updated scheme, the rate constant can be determined as in (76).

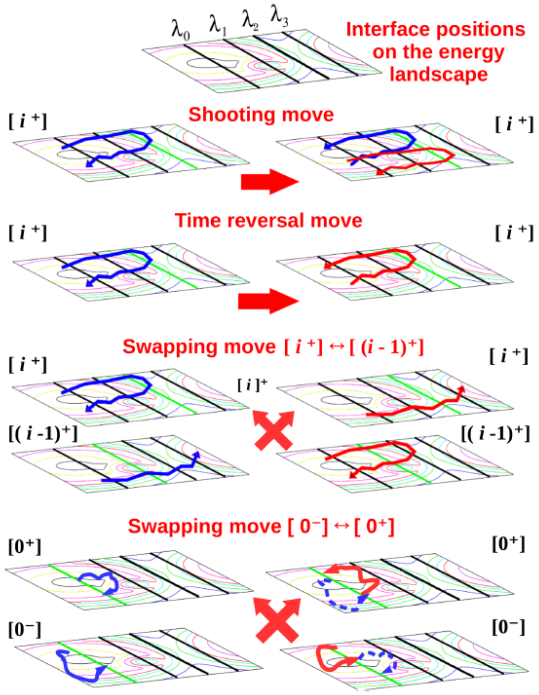

Figure 7: Schematic depiction of the shooting, time reversal and swapping move used in RETIS shown on a 2-dimensional free energy landscape with 4 interfaces $\lambda_0 - \lambda_3$. The green interface defines the crossing condition, blue paths represent old paths whilst red paths represent new paths. For the $[0^+]$ and $[0^-]$ ensembles, the start point of an old $[0^+]$ path becomes the endpoint of a new $[0^-]$ path which is grown backwards in time until reaching λ_0, and vice versa. Picture from Cabriolu et al. [48].

2.9 Wire fencing

A vital part of improving path sampling techniques is developing new moves that can efficiently sample trajectory space. The newest move under development is the *wire fencing* move. This move is depicted in figure 8. Between interface λ_n and λ_{n-1} there is a placed a cap. To sample a new path in the i^+ ensemble, the algorithm uses the time slices of the old path that crosses λ_i. If the old path has multiple segments that crosses λ_i, a segment is chosen at random proportional to the amount of time slices above λ_i. Once a segment has been chosen, the algorithm then picks a random time slice out of the segment which serves as the starting point new sub-trajectories. Small trajectories are then grown forwards and backwards time from the randomly selected time slice until either both directions reach λ_i, or the forwards reaches λ_{i+1} (or the cap) and the backwards reaches λ_i. This sub-trajectory can then be grown again according to the same procedure. After a set amount of sub-trajectories have been created, the last sub-trajectory will then be integrated forwards and backwards in time to create a full trajectory. The advantage of using this move is that by creating many sub-trajectories, the new path will be more decorrelated with the old path than if we were using the shooting move. The acceptance criterion for the wire fencing move is contingent upon the amount of points above λ_i in the old and new path as such:

$$P_{acc} = \left[1, \frac{\#points(o)}{\#points(n)}\right] \tag{80}$$

Rejection due to (80) can be avoided due to a technique known as "high acceptance". Here, every path is reweighted with a factor based on the amount of points in the trajectory and whether the path ended in A or B. If the trajectory is a $B \to A$ path, it can be accepted after being inverted in time. This makes it so that only paths that are $B \to B$ will be rejected, and the reweighting factor can be adjusted after sampling by unweighting to yield correct weights [49].

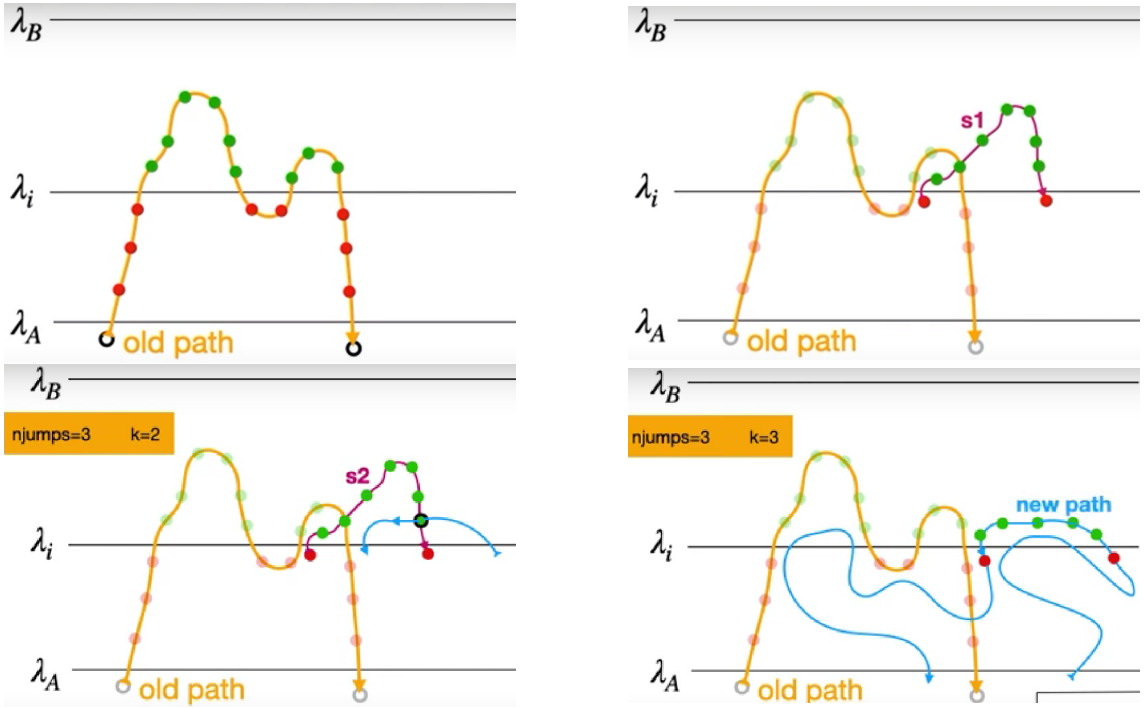

Figure 8: Depiction of the wire fencing move. Upper left: An old path with green points indicating segments above and red points below λ_i. Upper right: A random green point is picked and a new sub-trajectory $s1$ is generated until it reaches λ_i in both directions. Lower left: Another random point is picked from $s1$ and a new sub-trajectory is generated. Lower right: After a set amount of sub-trajectories, the last sub-trajectory is generated to create a full trajectory.

2.10 CdSe Nanocrystals

In order to demonstrate the previously discussed methods of harvesting transition paths, we turn to nanocrystals of CdSe. This system at ambient conditions possesses an equilibrium wurtzite structure which is 4-coordinated and hexagonally packed. However, at high pressures the structure changes into a 6-coordinated cubic rocksalt formation. Experimentally, this structural change has been shown to happen at pressures of about 2.5 GPa in bulk semiconductors [36]. However, since nanocrystals possess a size of a few nanometers, this pressure is not comparable to bulk material since the surface free energies of the two crystals are different. This means that the pressure needed to induce a transition is notably higher since the crystal size is smaller [17, 19]. The free energy barrier separating the wurtzite and rocksalt conformation can be defined in terms of activation energy and volume which strongly depend on both the size of the crystal and pressure. This indicates that structural change happens by lone nucleation and subsequent growth [20, 27, 31, 35].

In addition to the two stable structures, there exists a metastable structure, the 5-coordinated h-MgO structure. This intermediate structure is extremely short lived when transitioning with high pressures in MD, and its formation and existence depends on several factors, such as the shape of the initial wurtzite crystal and the transition pressure applied[43]. Lervik et al. [55] studied how the pressure and defects in the crystal impacted the transformation and found that the intermediate h-MgO structure is particularly long lived on the atomistic time scale for pressures between 4-6 GPa. In addition, Alivisatos et al. [19] discovered that spherical crystals that possessed disordered surfaces rarely lingered in the intermediate h-MgO structure, whilst faceted crystals with stable surfaces usually favoured to remain in h-MgO for a brief period of time before transitioning further to rocksalt. This leads us to conclude that favourable surface free energetics is the most important factor in the formation of the intermediate metastable structure. Here, computer simulations play a vital role in the identification of transformation mechanism in the crystal, since experiments often cannot provide information on the atomistic scale. Further, the intermediate structure is not

favoured in bulk material, but is relevant when dealing with nanocrystals, so information must be gathered with path sampling. Figure 9 depicts all three structures. The hexagonal structure of the wurtzite structure carries over into the h-MgO structure, however the puckered (001) layers are flattened, compressing the crystal.

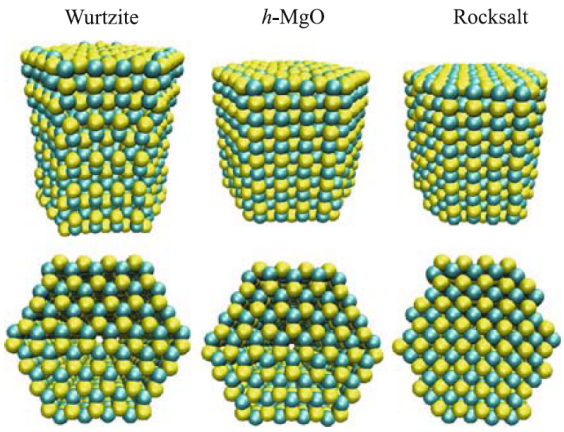

Figure 9: The three different structures of a $Cd_{528}Se_{528}$ faceted crystal. The crystals are viewed from the side and downwards the hexagonal c-axis. Figure from Grünwald and Dellago [43]

To perform path sampling on the transition of wurtzite to rocksalt, one has to use a suitable OP λ which can distinguish between wurtzite and rocksalt, as well as h-MgO since the structure is metastable for a small time regime. One intuitive solution is to use the fractional coordination number of the crystal, since each structure has a different coordination number. However, this poses problems as a less than perfect crystal will have multiple atoms where the coordination number does not conform to the structure of the crystal. In an MD simulation or a TPS simulation, the temperature and pressure imposed will most certainly create impurities in the crystal, either during equilibration or during the actual path sampling. The simpler solution to the OP problem is to use the volume of the crystal, calculated as the size of the simulation box at any given time. By running an MD simulation where the transition occurs, one can find the volume of the rocksalt structure which will be λ_B, and the volume of the wurtzite structure which will be λ_A.

3 Experimental

3.1 Molecular Dynamics initialisation

The start point was a Molecular Dynamics simulation of a 2048 atom CdSe crystal ($Cd_{1024}Se_{1024}$) to create an initial path for the path sampling simulation. The crystal was made by growing a triclinic unit cell of Cd_2Se_2 in Avogadro[45] as shown in figure 10, 8 times in each direction in a 3-dimensional coordinate system yielding 512 unit cells. The crystal could now be used as the starting configuration for MD simulations. The interatomic interactions were modeled by using the interatomic pair potential for the CdSe system developed by Rabani [32]. The Coulombic interactions were computed with the smooth particle mesh Ewald (PME) method[18] with a cut-off of 1.0 nm and van der Waals interactions were truncated at 1.0 nm and dispersion corrections were applied to the energy and pressure. Periodic boundary conditions were applied in all directions and the system was anisotropically coupled to the Berendsen barostat[10] with a coupling parameter of 4 ps. The Parrinello-Rahman barostat is unsuitable to this system as it is subject to fluctuations in volume that spans the range $\lambda_A - \lambda_B$, creating trajectories that seemingly transitions between the two states. The system was also coupled to a velocity-rescale thermostat[40] with a stochastic element at 300 K with a coupling parameter of 0.5 ps. The velocity-rescale thermostat was selected as it samples the exact canonical distribution. The mass motion center was removed linearly every 100 steps to prevent the system from drifting.

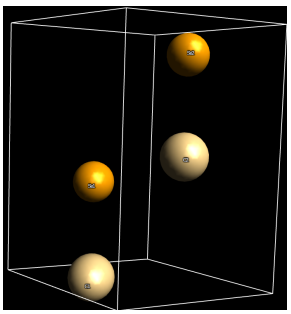

Figure 10: A single unit cell of Cd_2Se_2 created with Avogadro [45].

The system was first energy minimised and then equilibriated in the NVT and NPT ensemble respectively. This produced a plane defect in the form of a ring formation which is from here on denoted as plane defected crystal (PDC). Another crystal was then created similarly, but restricted entirely to the simulation box to create a defect free crystal (DFC). After the systems were stable at ambient conditions, brute-force MD was ramon the systems at 300 K and 1000 K with varying pressures to study the effect of temperature on the transition and to find the transition pressure for each crystal. To select an appropriate λ_0 interface, a long MD simulation (1 ns) was ran at the target pressure of each crystal to discover the equilibrium fluctuation which is shown in figure 11.

3.2 Initial path creation

The target pressure was set 1 GPa under the transition pressure for easier sampling. The transition pressure for the DFC was 11 GPa and for the PDC it was 9 GPa. The initial path for path sampling was created for each system by splicing a transitioning MD trajectory at the transition pressure for each system with a multiple MD trajectories that had been carried out at the target pressure and intermediate pressures between the target and transition pressure. This yielded a rather undynamical path, which is not usually a problem since within a number of MC moves, the algorithm will sample more likely dynamical trajectories according to the Boltzmann distribution. The initial trajectory also had the advantage of remaining for a relatively long time in A (wurtzite) which is necessary for ergodic sampling of phase-space. Negative volume per particle was then chosen as the OP λ to separate wurtzite and rocksalt as the algorithm needs to proceed along a positive change in λ. The initial trajectory for the defected system is shown in figure 12.

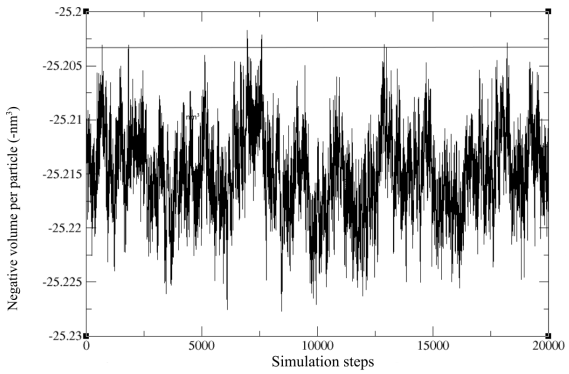

Figure 11: 1 ns MD equilibration for determining λ_0 at 10 GPa with the DFC. The blue line represents λ_0.

3.3 RETIS settings

GROMACS [47] was used as the MD engine for the simulation with the initial structure as a wurtzite structure at ambient conditions and the topology described by the interatomic pair potential of Rabani [32]. GROMACS ran with a timestep of 0.002 ps and 5 subcycles, meaning the amount of steps GROMACS simulates before λ is recalculated. The max length of 20 000 steps was never hit, meaning that the subcycles parameter did not have an effect on the results since all paths were completed before reaching the step limit. The target pressure was set to 10 GPa for the defect-free crystal, 1 GPa below the transition pressure. Figure 11 was used to determine a value of λ that the simulation crossed several times and was outside the typical equilibrium fluctuations. The straight line at $\lambda = -25.202$ represents λ_0. Figure 12 shows the initial trajectory with several interfaces and λ_B at the point of no return $= -24.8$, where the transition probability is ≈ 1. The interface cap for wire fencing was put at -24.83 with the number of jumps set to 6 with time reversal frequency at 0 and swapping frequency at 0.5. Initial paths for each ensemble were loaded in from an existing path with the blue line in figure 12 being the initial path for all ensembles $\neq [0^-]$, and the green line for $[0^-]$. This trajectory jumps drastically in volume, however it is not necessary for initial paths to be dynamical in nature so this effect can be neglected.

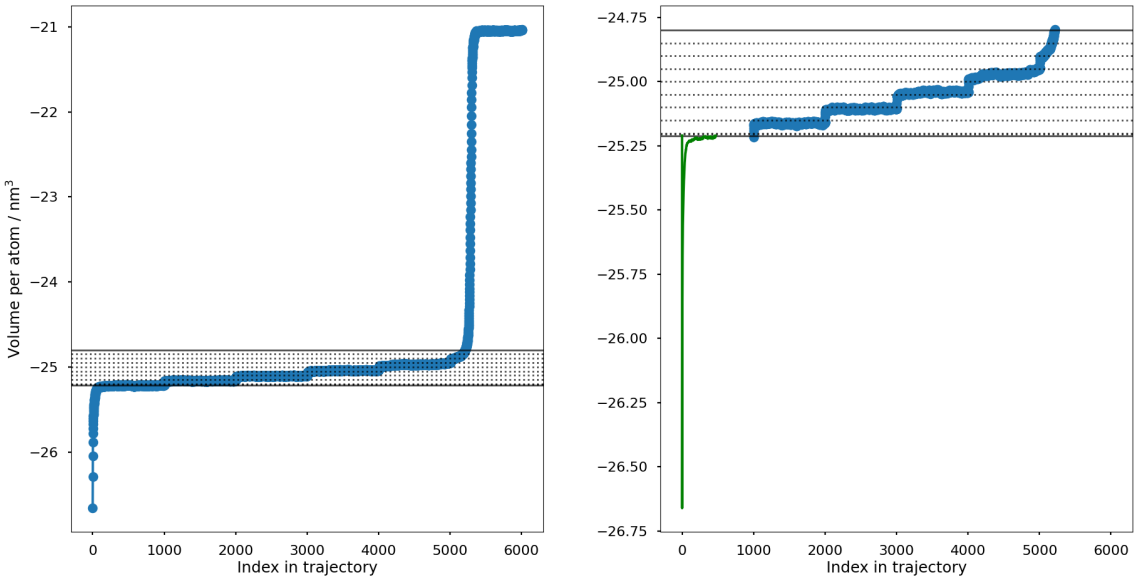

Figure 12: An initial trajectory initialised with several intermediate equilibrium pressures. The order parameter is negative volume per particle, so the volume is multiplied with -1 so that the reaction progresses from a low to high value.

4 Results & Discussion

The results & discussion section has been split into the following two sections: an MD simulation results and a rare events results. In the MD section, results are presented in terms of structure of the DFC and the PDC. Then the effect of pressure and temperature on the system is discussed before discussing the total energy and Gibbs free energy difference between structures. In the rare events section, issues with creating an appropriate initial trajectory are presented as well as the issue of "energy switching" where trajectories fluctuate drastically between short and long paths. Next, the placement of interfaces in trajectory space is discussed as well as presenting results from the wire fencing move. Lastly, crossing probabilities for the shooting and wire fencing move are presented.

4.1 Molecular Dynamics

4.1.1 Crystal defects & structure

Figure 14 shows two CdSe crystals that was energy minimised before being equilibriated in the NVT ensemble and in the NPT ensemble. One crystal was not restricted in any way during the equilibriation which produced a stable crystal with a plane defect down the (001) axis, a ring formation as can be seen in figure 14b. Since a standard MD equilibration readily produced this defect, it is fair to assume that this defect may be common in nanocrystals at ambient conditions. Therefore, it is of interest to further study this defect to see how it affects the transition from wurtzite to rocksalt. Note that the force field parameters by Rabani [32] has not been optimised for crystals with defects which can lead to undynamical results. Lervik et al. [55] tested the forcefield on the CdSe system with a DFC and found that the energies provided where acceptable when compared to density functional quantum chemical calculations. The other crystal was restricted to the simulation box at all times to produce a defect free crystal as shown in figure 14c and 14d. Although both figure 14a & 14c seem to indicate that there are few Se atoms irregularly scattered across the top layer of the crystal, this is due to how GROMACS calculates atoms within the simulation box, and for simulation purposes they are included in the integration of motion through periodic boundary conditions. The final structure of the rocksalt formation did not change between the defected and the defect free crystal, indicating that impurities in the wurtzite structure are not significant for the final shape of the rocksalt structure. The shape of the rocksalt crystal is shown in figure 13.

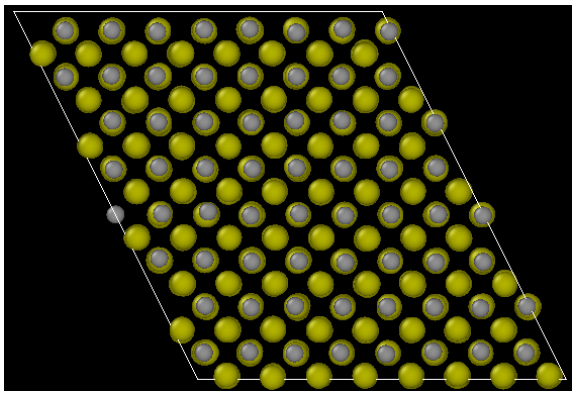

Figure 13: Rocksalt structure of the CdSe crystal viewed along the (001) axis.

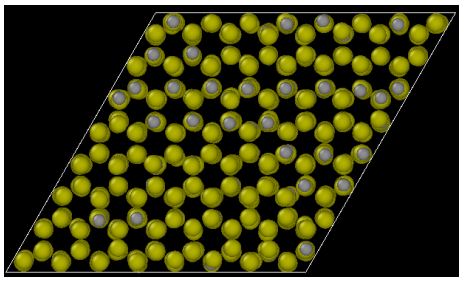

(a) PDC faceted CdSe crystal seen down the (001) axis.

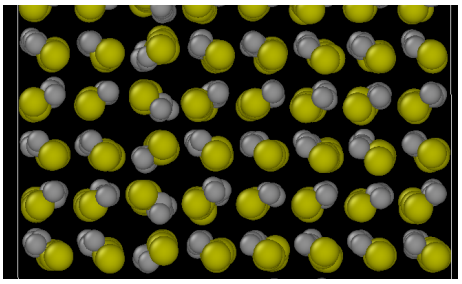

(b) PDC faceted CdSe crystal seen along the (010) axis.

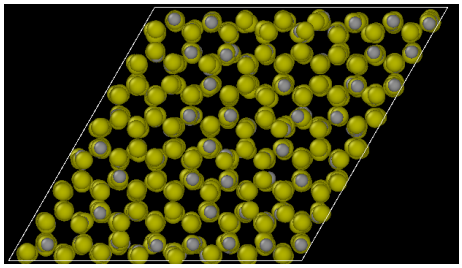

(c) DFC faceted CdSe crystal seen down the (001) axis.

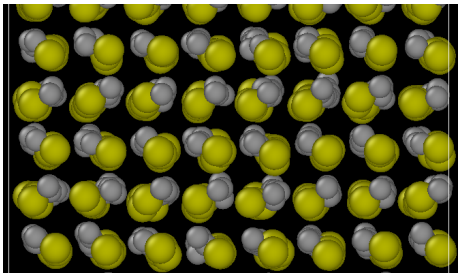

(d) DFC faceted CdSe crystal seen along the (010) axis.

Figure 14: PDC and DFC CdSe crystals. Yellow spheres are cadmium and grey spheres are selenium. The white lines around the structure indicate the simulation box.

4.1.2 Pressure and Temperature effects

Figure 15 shows the volume as a function of pressure of the DFC at 300 K and the PDC at 300 & 1000 K. As the pressure increases, the volume of the crystal drops regardless of the crystal structure. This is expected, as increasing pressure compresses the crystal. Notice that regardless of the temperature, the transition pressure was in the region of 9 GPa for the PDC. This indicates that temperature is not a driving factor in facilitating the transition from wurtzite to rocksalt. Therefore, simulations at 300 K are more reasonable to carry out since they are closer to experimental conditions. Therefore, the DFC at 1000 K was not studied as the structure is more stable and thus unlikely to provide any meaningful insight. The transition does not happen spontaneously for either crystal structure between $2 - 8$ GPa for the simulated time. This is expected as at experimental conditions the transition happens at 5 GPa[17]. Therefore, it is expected that for pressures > 5 GPa a transition will be observed given a long enough MD simulation. With the DFC, the system does not transition until pressures of 11 GPa are introduced. The volumes given for the DFC are in agreement with the results obtained by Lervik et al. [55].

These results indicate that the plane defect in the CdSe crystal lowers the potential energy barrier for transitioning drastically. The plane defect thus introduces an instability in the crystal that facilitates nucleation provided that the pressure is sufficient. This instability also has the potential to induce multiple nucleation centers, facilitating quicker transition. A perfectly ordered crystal without impurities that cause instability lowers the probability of a nucleation center due to the high potential energy barrier, and thus higher pressures are required to transition. Figure 16a shows the volume of the DFC over 60 ps at the transition pressure (11 GPa), whilst figure 16b shows the volume of the PDC over 60 ps at its transition pressure (9 GPa). The DFC clearly shows a plateau at $\approx 51\ nm^3$ before reducing to the second plateau at $\approx 43\ nm^3$. Coordination analysis revealed that at the first plateau, a majority of atoms in the crystal were 4-coordinated, corresponding to a wurtzite structure. The second plateau is then the volume at the rocksalt structure. For the PDC, this wurtzite plateau was not reached, instead the system favoured a direct transition into rocksalt. In both figures, the sudden drop in volume at the start of simulation is due to the system being initialised at ambient conditions.

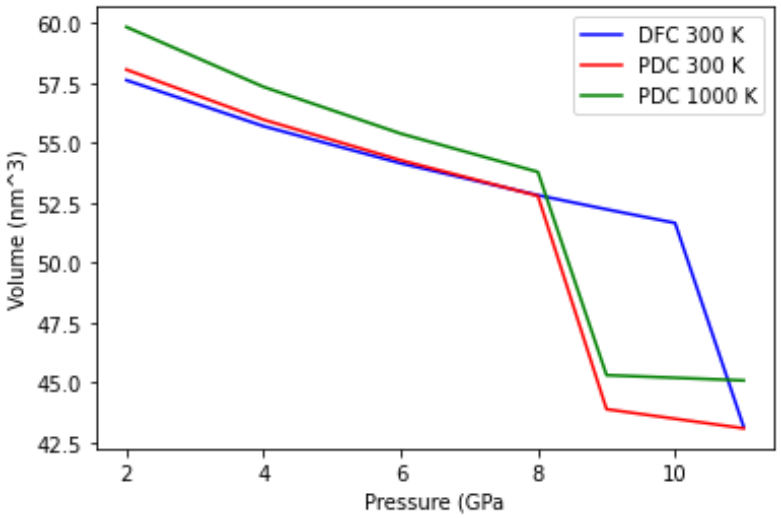

Figure 15: Volume of the DFC at 300 K, the PDC at 300 K and the PDC at 1000 K.

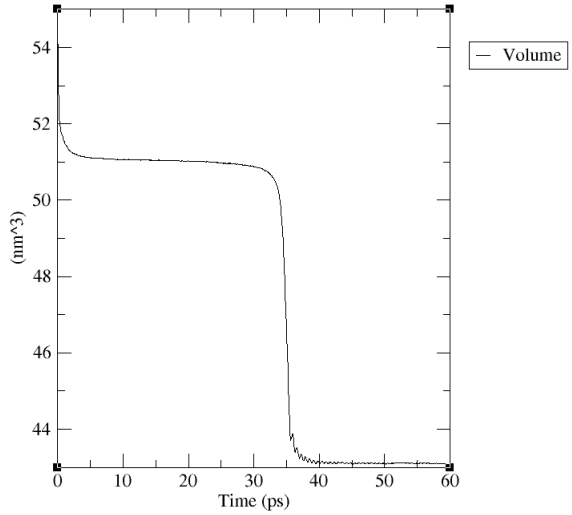

(a) Volume of the DFC subjected to 11 GPa at 300 K.

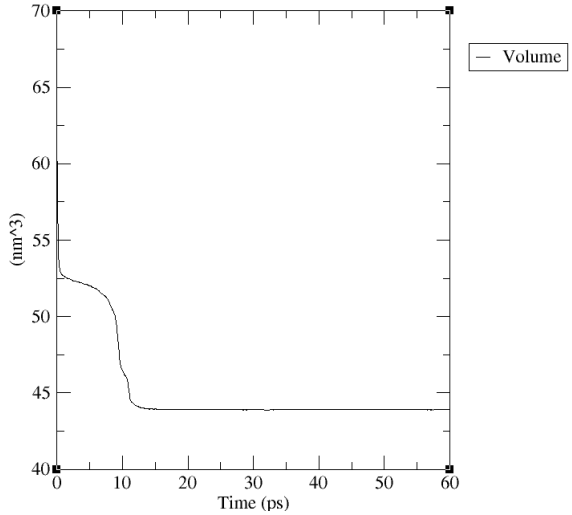

(b) Volume of the PDC subjected to 9 GPa at 300 K.

4.1.3 Total energy

Figure 17 show the total energy of the DFC, PDC and rocksalt structure as a function of pressure. As expected, the total energy rises with the pressure, as the compression of the crystal brings the atoms inside the crystal closer together. This increases the potential energy as the electromagnetic interactions between atoms are pushed out of equilibrium, giving rise to tension. Also note that the energy of the PDC crystal is higher than the DFC, indicating that it is less stable. This is consistent with the fact that the PDC has a lower transition pressure than the DFC. The sudden change in the PDC's energy of $+11 \cdot 10^3$ kJ/mol between 8 & 9 GPa is due to the transition between wurtzite and rocksalt. From 10 GPa to 11 GPa in the DFC, the energy change is $+7 \cdot 10^3$ kJ/mol. This is a larger change in energy than between any pressure change in the wurtzite structure for either crystal, which is consistent with the tight packing of the rocksalt structure. Since it is a 6-coordinated cubic crystal structure, the potential energy is expected to be noticeably higher than in the wurtzite structure, where the 4-coordination of the crystal provides more empty space between each atom. Figure 18 shows the total energy of a transition simulation for the DFC and PDC. The transition barrier for the PDC is notably higher than the one for the DFC. This is due to the potential energy of the PDC being higher due to the irregular structure of its crystal, giving rise to tension. The DFC can be seen to have a stable state for 30 ps in the simulation, providing further evidence that the DFC is the more stable crystal structure.

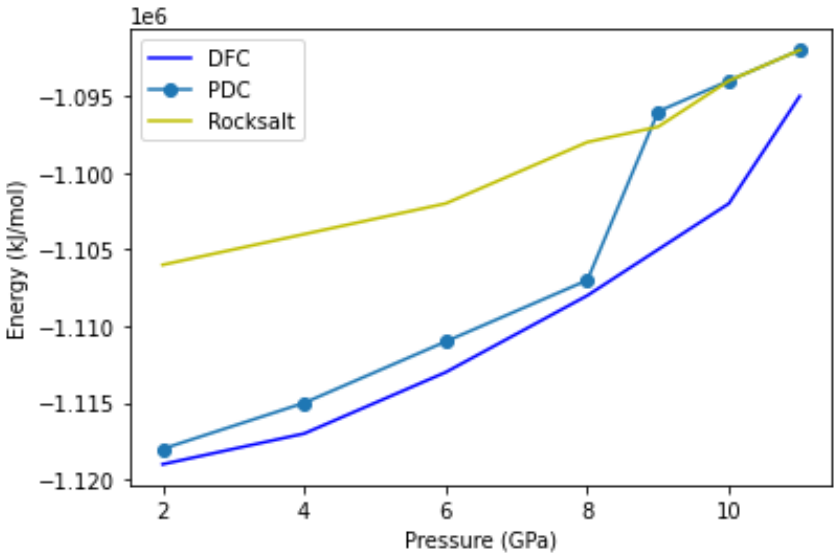

Figure 17: Total energy plot of the DFC, PDC and rocksalt structures as a function of pressure.

Any system will transition into the state where the Gibbs free energy is the lowest. Gibbs free energy $G = H - TS$ where H is the enthalpy, T is the temperature and S is the entropy. The difference in crystal structure between wurtzite and rocksalt is not so radical that a large change in entropy is expected, therefore at constant temperature the enthalpy determines which state is the most stable. $H = U + pV$ where U is the internal energy and pV is the pressure-volume energy term. These properties are plotted in figure 19. The change in enthalpy is linear and proportional to the energy change for the both crystal structures. The enthalpy of both the DFC and PDC are similar for the wurtzite structure as well. The pressure-volume energy exhibits the same pattern as enthalpy, however when transitioning to rocksalt the energy is lower i.e. more stable than the preceding wurtzite structure. Finally, looking at the internal energy shows that the PDC naturally possesses a higher energy than the DFC when in the wurtzite structure, providing further evidence that the PDC is a less stable configuration.

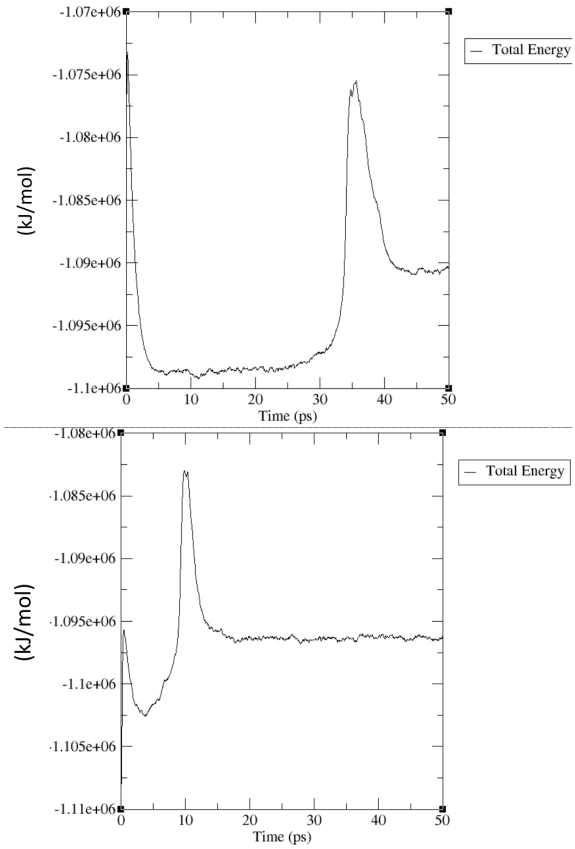

Figure 18: Total energy of the DFC (upper) and the PDC (lower) as a function of time at their respective transition pressure.

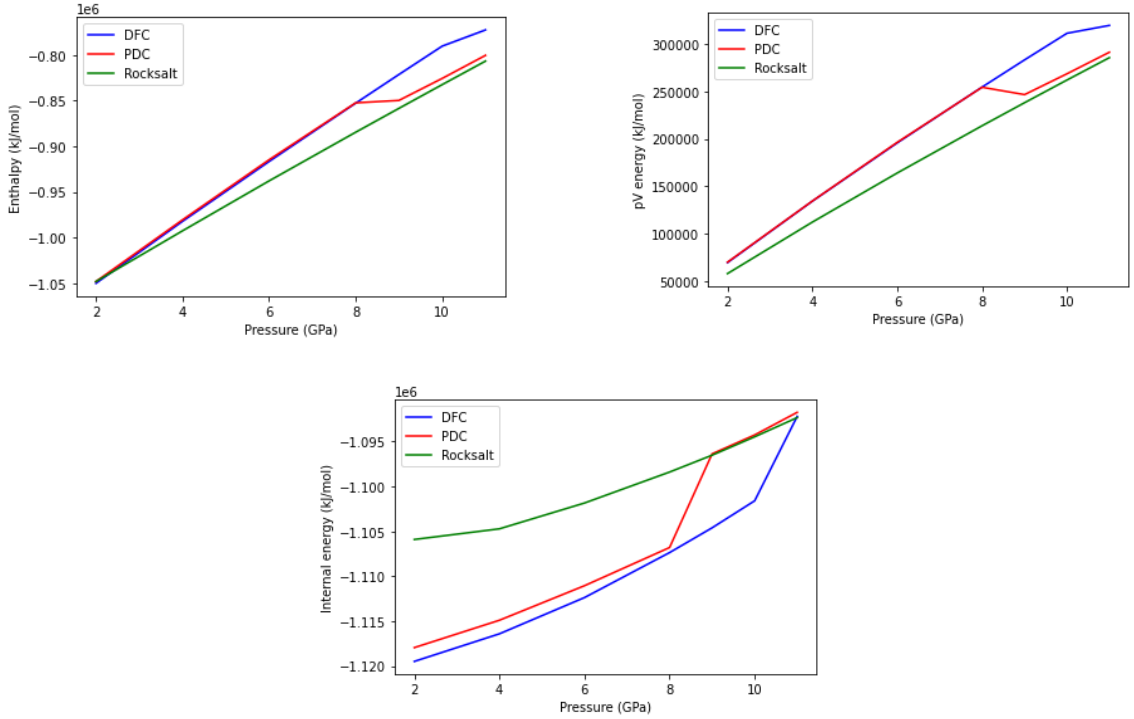

Figure 19: Enthalpy, pressure-volume energy and internal energy plotted against pressure.

4.1.4 Transition

Figure 20 and 21 depicts two crystals, DFC and PDC respectively, at the moment of transition. Nucleation begins at the edges of the crystal and subsequently grows into a rocksalt structure along a line in the crystal. The instability caused by nucleation causes the rest of the crystal to transition as well, creating an ordered rocksalt structure. There were no grain boundaries or defects in the rocksalt structure, although this is probably due to the rather small crystal size. If the system was larger, say closer to bulk CdSe, then the probability of grain boundaries and defects would increase. Also of note is the intermediate h-MgO structure that can be observed in both crystals. The structure was short-lived and collapsed almost immediately, but coordination analysis at this time slice revealed almost all atoms to be 5-coordinated. Lervik et al. [55] studied a similar system with 1024 atoms. However, this system showed no sign of nucleation, only a concerted motion of atoms transitioning between the structures. Naturally, the probability of nucleation increases with crystal size as there is more surface and areas that the nucleation can start from. This also indicates that the number of atoms needed to observe nucleation is in between 1024-2048.

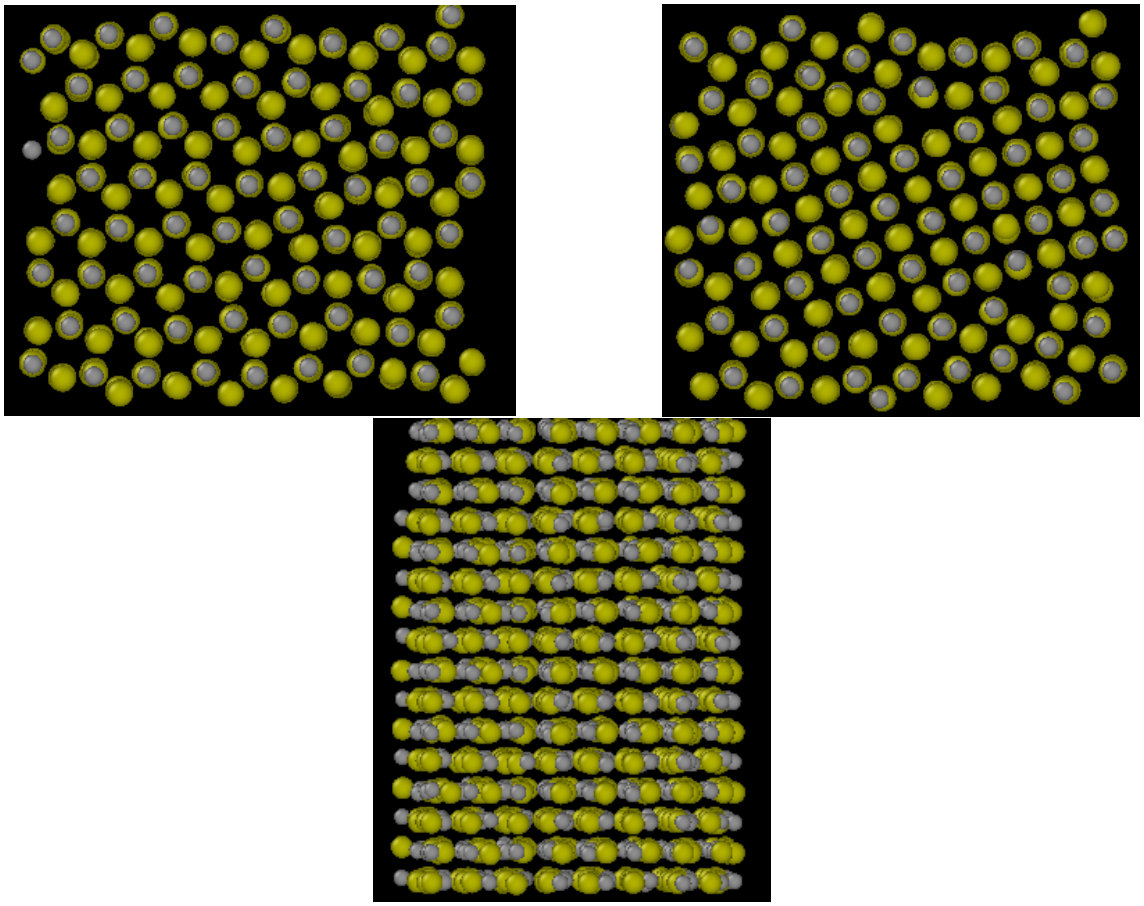

Figure 20: Snapshots of a transitioning DFC crystal. Upper left: Nucleation begins and makes the crystal unstable. Upper right: Rocksalt formation along a line in the middle of the crystal. Bottom: The h-MgO intermediate structure at transition.

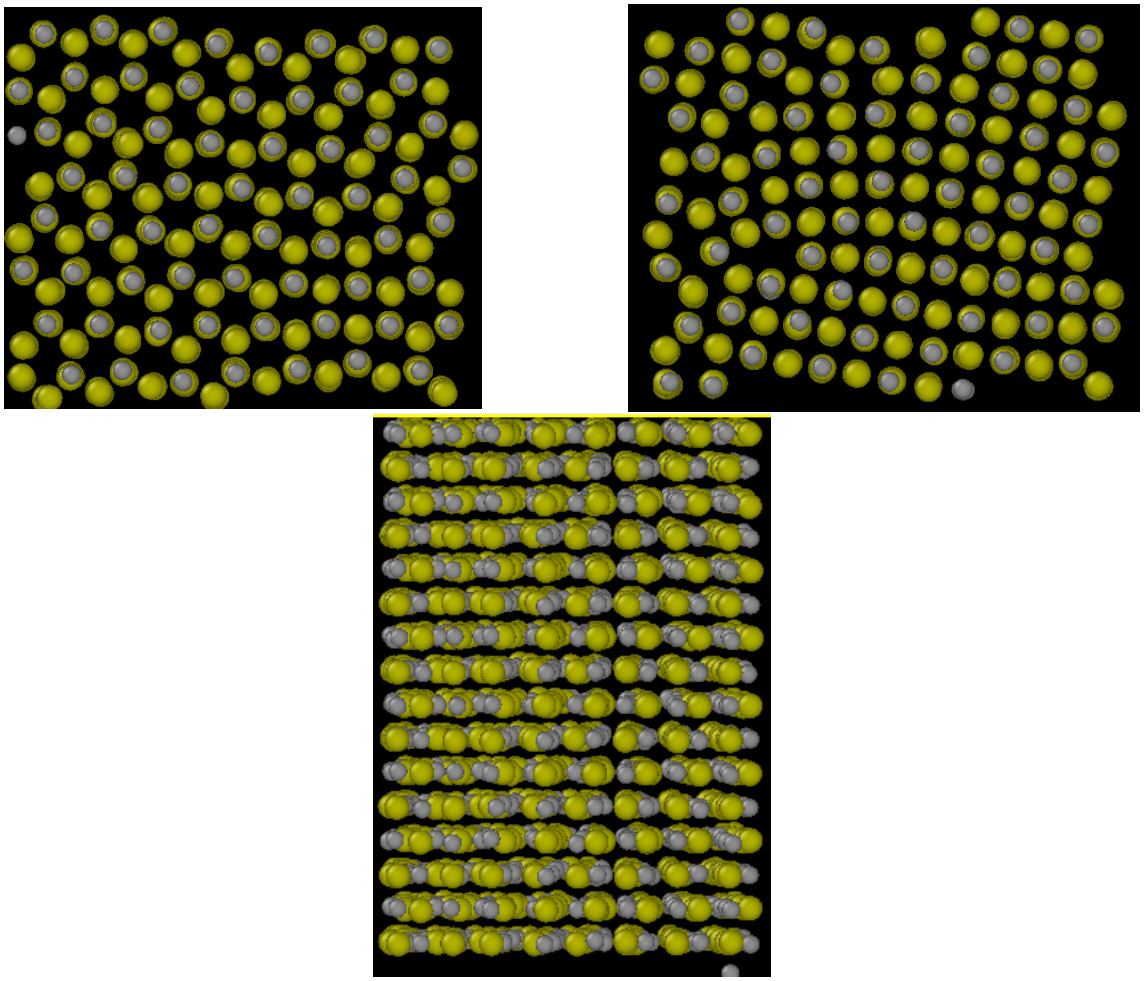

Figure 21: Snapshots of a transitioning PDC crystal. Upper left: Nucleation begins and makes the crystal unstable. Upper right: Rocksalt formation along a line in the middle of the crystal. Bottom: The h-MgO intermediate structure at transition.

4.2 Rare events

4.2.1 Initial trajectory issues

A challenge of performing path sampling is creating a decent initial trajectory for the algorithm. As discussed in section 2.4, an initial trajectory does not necessarily need to be dynamical. As long as the initial trajectory is reactive (connects A and B) and provides a sufficient definition of A, the trajectory should give rise to dynamical trajectories after a number of MC moves. There are several ways to create an initial trajectory, the first and most intuitive being to run a long enough MD simulation where in the rare event takes place. However, this is difficult to achieve with either crystal as for low pressures the chance of spontaneous transition is extremely small, meaning an extremely long MD trajectory might never observe a transition, thus making this a very costly approach. One could remedy this issue by increasing the pressure in the MD simulation, but doing so alters the equilibrium volume of the wurtzite structure as can be seen in figure 15 Therefore, an initial trajectory obtained at one pressure cannot be directly used when sampling at a different pressure. To solve this issue, an MD simulation was ran at a pressure where the system would transition. Then, a second simulation was ran at the target pressure which did not transition. This gives us two separate trajectories which can be spliced together in order to create an undynamical path which is both reactive and has a well-defined A. This initial trajectory is shown in figure 22. However, depending on the free energy landscape, an undynamical path might give rise to a path sampling simulation that needs many MC moves before it starts sampling dynamical trajectories.

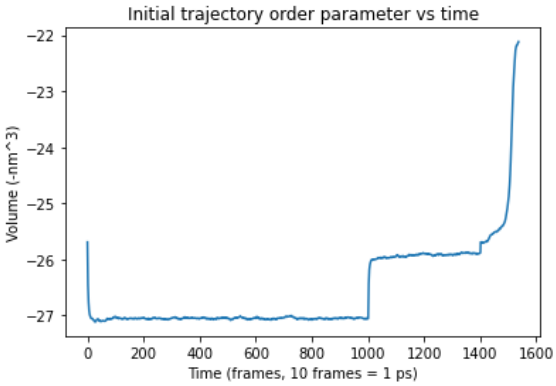

Figure 22: Initial trajectory for RETIS simulation with the order parameter (negative volume per particle) plotted against the time frames of the spliced trajectories.

4.2.2 Energy switching

A common problem that was encountered when utilising an artificial initial trajectory such as figure 22 was the switching between short and long trajectories. Figure 23 shows trajectories of a simulation with figure 22 as the initial trajectory in the $[0^-]$ and $[0^+]$ ensemble, respectively, for a simulation with two interfaces $\{\lambda_0, \lambda_1\}$. Both ensembles exhibit a pattern of shooting and swapping between a long path and a short path. For the $[0^-]$ and $[0^+]$ ensembles, shooting and swapping are similar in that they both integrate the equations of motion, as opposed to swapping for ensembles $\neq \{[0^-], [0^+]\}$ which switches existing paths between ensembles given that they fulfil the criteria of that particular ensemble. The difference between shooting and swapping in the $[0^-]$ and $[0^+]$ ensembles is that the shooting modifies the conditions at the shooting point, whilst swapping provides the engine with the start or end points of new trajectories on the boundary of λ_0. Of interest here is also the relative energy of the short and long paths in each ensemble. The short path has a higher average energy than a long path.

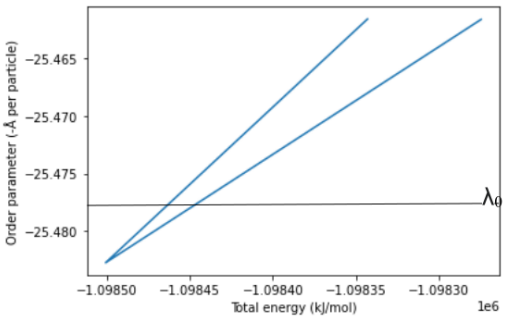

(a) Short trajectory in the $[0^-]$ ensemble.

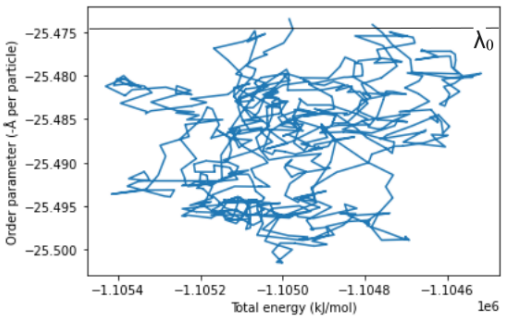

(b) Long trajectory in the $[0^-]$ ensemble.

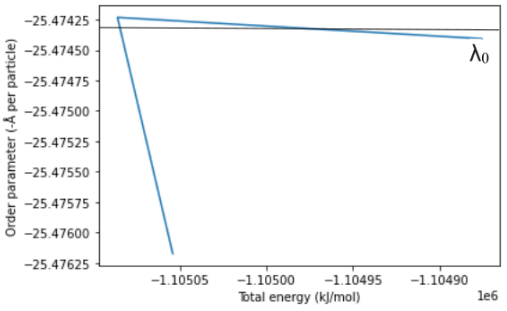

(c) Short trajectory in the $[0^+]$ ensemble.

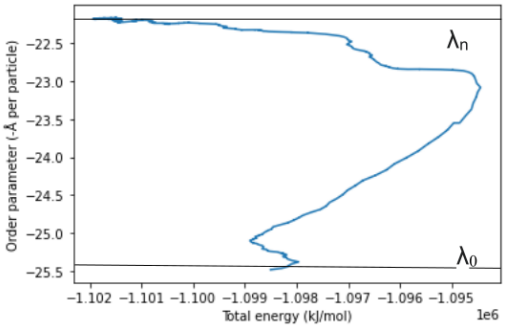

(d) Long trajectory in the $[0^+]$ ensemble.

Figure 23: Short and long trajectories switching between the $[0^-]$ and the $[0^+]$ ensemble.

This is an example of the system encountering some form of sampling trap. It should be noted that the system was simulated for 14 days and generated only 50 cycles. This indicates that the simulations are quite costly due to the generation of long trajectories that are undynamical in nature. It is expected that dynamical trajectories in the $[0^-]$ ensemble are longer than trajectories in the $[0^+]$ ensemble due to the system fluctuating in A before returning to λ_0. This behaviour is reflected in the energy of the long trajectories in both ensembles, as the energy in $[0^-]$ is fluctuating constantly around an equilibrium, whilst in $[0^+]$ the energy is high when surpassing an energy barrier separating the stable states, before lowering when relaxing into either A or B. The energy behaviour of the short paths indicates that in the $[0^-]$ ensemble, short paths are initiated with a high energy, immediately forcing the system back to λ_0 which creates an undynamical short path. In the $[0^+]$ ensemble on the other hand, short paths are initiated with low energy which is insufficient for breaking away from the basin of attraction of A, leading to immediate relaxation back into A. What this indicates is that paths are swapped between low and high energy, causing short and long paths every other move that requires integration.

4.2.3 Interface placement

Figure 22 shows a typical initial transition path. In order to successfully place interfaces, the boundaries of A and B must be discovered as well as the areas in which the probability to progress along the order parameter is small and where it is large. An equilibration MD run carried out over 1 ns is often sufficient to stabilise the system at the target pressure. A high boundary of the fluctuation peaks can then be selected as λ_0 so that most of the trajectory is contained within A. λ_B can be placed at the steep hill leading to the rocksalt configuration, as the system will always transition into B. This makes it so that the simulation will reach λ_B in a smaller amount of steps while still preserving the ensemble distribution, leading to more efficient sampling.

One issue that presented itself when employing the shooting move was the low amount of accepted paths in the ensembles close to λ_B. This indicates that reaching λ_B is naturally difficult when below the transition pressure, which is to be expected. This makes setting an efficient amount of interfaces close to B harder, as interfaces are optimised for sampling after the initial path effects are gone. A few ensembles produced many rejected paths with the "backwards wrong interface" (BWI) label. This means that the backwards integration from the shooting point ended up in B. This is an indication that paths in this ensemble are shot from within the basin of attraction of B, and therefore the interfaces corresponding to these ensembles can be removed which subsequently moves λ_B further to the left. For the ensembles which truly lie below λ_B, obtaining a path that transitions from A to B, as opposed to one that starts and ends in A, is often quite difficult. Table 1 shows the placement of interfaces for the DFC in a 10 GPa RETIS simulation. More interfaces was put close to λ_A since breaking away from A was difficult and so multiple interfaces was put there after inspecting the path ensembles. After this, the spacing between A and B was uniform.

λ (Volume per particle $-nm^3$)
-25.212
-25.205
-25.203
-25.15
-25.1
-25.05
-25
-24.95
-24.9
-24.85
-24.8

Table 1: Interface placement along the OP for the DFC at 10 GPa.

4.2.4 Wire fencing

The idea behind the wire fencing move is that paths can be decorrelated faster by creating small sub-trajectories between interface λ_i and the cap $\lambda_{cap} < \lambda_B$. As this move is yet to be tested properly so that the parameters can be optimised, 6 sub-trajectories was selected. This resulted in sub-trajectories that often had issues in travelling far from the interface it was issued from. More sub-trajectories naturally increases the cost of each move, however it can be useful to ensure decorrelated trajectories. After 45 cycles, all trajectories using the wire fencing reaches the same maximum along the order parameter. Further inspection of the trajectories reveal that every full trajectory generated after the sub-trajectories only slightly surpass λ_i before returning to A. This did not result in rejected trajectories. Wire fencing moves have a naturally high acceptance rate, even without utilising high acceptance, since the final trajectory is always initiated from above λ_i for ensemble $[i^+]$, so there are zero rejections for no crossing with λ_i.

Another issue with the wire fencing move presents itself in the creation of an initial path. In order for a wire fencing move to be performed, there has to be a certain amount of time slices above the interface λ_i and the interface cap. Figure 24 shows an initial trajectory with $\lambda_A = -25.212$ at 10 GPa and $\lambda_B = -24.8$, the point of no return. This initial trajectory was made using the simple procedure of splicing an equilibrium trajectory at the target pressure with a reactive trajectory at the transition pressure. Note that early on past λ_0 there are no time slices. This is due to the sudden shift in pressure between the two trajectories, causing the system to contract quickly during the initial steps, making it so that the time slices above λ_A come from a trajectory with the energy necessary for transitioning to rocksalt. This means that the modification of any points configuration or momenta must be large enough to break away from the transition. However, the modification was usually not sufficient. This made it so that wire fencing moves were likely to be integrated in both directions into B, rejecting the trajectory altogether.

This problem can be remedied by creating multiple equilibrium trajectories at intermediate pressures between the target and transition pressure, such that the trajectory has more time slices above λ_A that are not from a transition trajectory. Naturally, this increases the size of the initial trajectory file, which in turn makes a simulation more costly due to initialisation of each ensemble. This is exemplified in figure 12. The initial path for the $[0^-]$ ensemble is the same, but the for all other ensembles, there are more time slices which can be used for a wire fencing move. Note that the length of the reactive path has increased in size from $\approx 450 \rightarrow \approx 4000$, almost an increase by a magnitude of 8. The simulation cost scales with both the number of interfaces and length of the initial trajectory. This becomes a problem which has an inversely proportional relationship with the probability of the rare event. Another issue that presented itself in the simulations lied in how GROMACS calculated volume for the OP. Inspection of order parameter files revealed that the simulation box volume was updated every 20 fs. This resulted in simulations where the order parameter was identical for every 2 steps, effectively increasing the length of trajectories since the volume is not updated correctly. This can be solved by updating the frequency of the barostat.

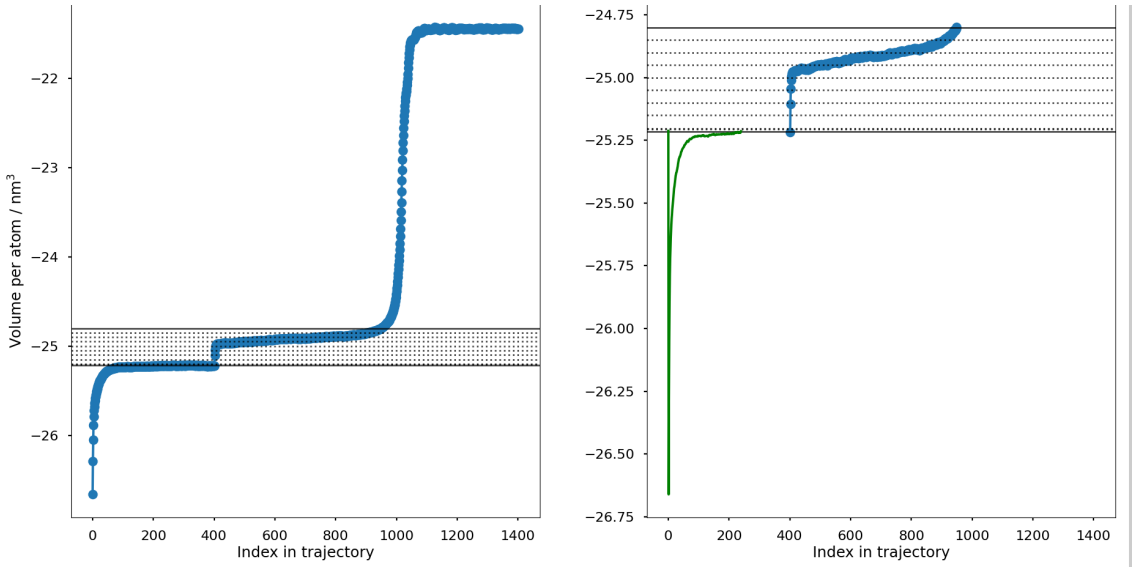

Figure 24: Left: An initial trajectory with λ_A at the bottom solid black line, λ_B at the top and all other interfaces marked with dotted black lines. Right: Green line represents initial trajectory in the $[0^-]$ ensemble, blue line represents initial trajectory for all ensembles $\neq [0^-]$. Dots indicate time slices.

4.2.5 Crossing probabilities

The conditional crossing probabilities between interfaces are vital to the success of RETIS as a tool for computing dynamical information. Figure 25 and 26 show the overall and matched probability of the shooting move and wire fencing move, respectively. The statistical outliers in trajectories shown in the left hand side of figure 25 comes from early trajectories that had not yet decorrelated from the initial path. Otherwise there are signs of convergence as the right hand image shows a gradually decreasing crossing probability. However, this is not yet fully converged as the graph should look like a smooth function when converged. Figure 26 shows that the system has issues converging when using the wire fencing move. This can be attributed to the move being under development, and such the parameters has not yet been tuned so that it effectively samples the system. However, there are no outliers in trajectories when using the wire fencing move due to the rapid decorrelation it provides. Due to the lack of convergence from the shooting move simulation, a reliable estimation of the rate constant was not found.

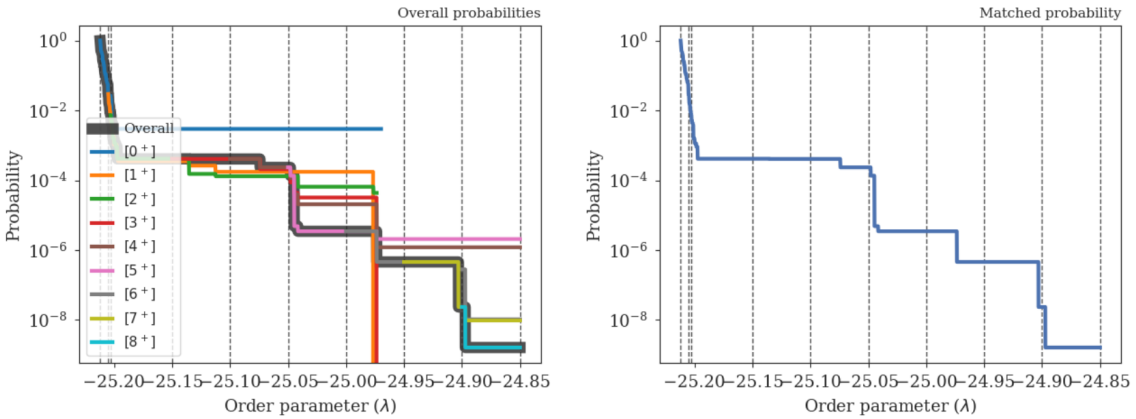

Figure 25: Overall and matched probability as a function of the OP λ for a simulation using the shooting move.

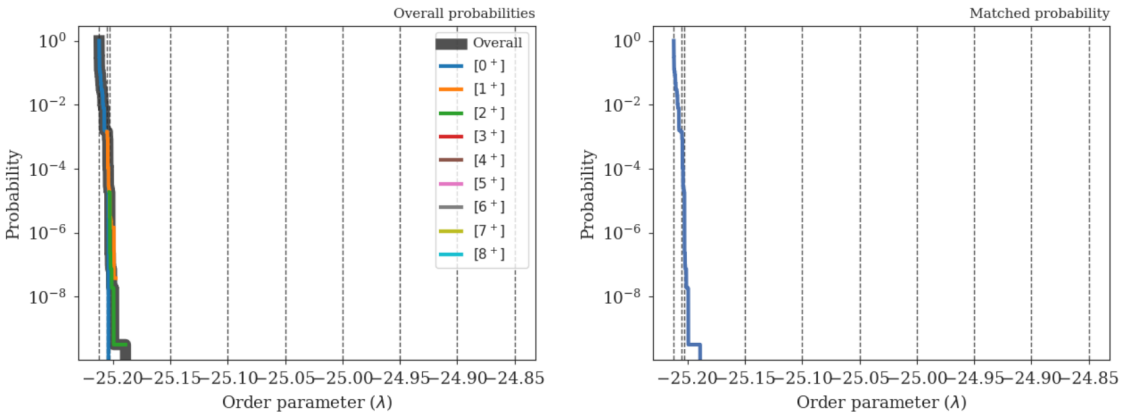

Figure 26: Overall and matched probability as a function of the OP λ for a simulation using the wire fencing move move.

5 Conclusion

MD simulations of the CdSe nanocrystal at ambient condition can readily produce a plane defect which lowers the stability of the crystal, leading to easier transitioning. The transition pressure for such a defected crystal in an MD simulation was 9 GPa whilst the transition pressure for a defect free crystal was 11 GPa. The 5-coordinated intermediate h-MgO structure could be observed briefly at the moment of transition for both crystals, and transition removed the defect from the crystal, making the rocksalt structure equal between both crystals. Wire fencing proved unsuitable to handle the system as the convergence was slow, however the trajectories generated decorrelated faster than trajectories produced by shooting.

6 Further development

Naturally, since the wire fencing move is an early development stage there are several parameters which has to be adjusted. By further testing of the system with varying amounts of sub-trajectories, one could find an optimal amount for efficient decorrelation of trajectories. This should however be regarded as a system specific, as the amount depends on the potential energy landscape the system resides in at any given time. Furthermore, the system can be studied with a reversal of stable states, that is rocksalt can be set as A since it is metastable at pressures lowers than the transition pressure, which could raise the probability of $A \rightarrow B$ transitions. The system can also be studied as a nanocrystal without periodic boundary conditions so that surface free energetic effects can be studied to determine the mechanism of transition, and how it differs from larger crystals with regards to pressure.

7 Acknowledgements

The computer simulations were performed on the IDUN cluster at the High Performance Computing Group at NTNU and at the Titus1 computer at the applied theoretical chemistry group at the department of chemistry at NTNU. I would also like to thank my supervisors Titus van Erp and Anders Lervik for enduring my minute questions regarding every matter technical and theoretical.

References

(1) Chandrasekhar, S. *Rev. Mod. Phys.* **1943**, *15*.

(2) Metropolis, N.; Rosenbluth, A.; Rosenbluth, M.; Teller, A.; Teller, E. *J. Chem. Phys.* **1953**, *21*, 1087–1092.

(3) Klein, M. *Phys. Rev.* **1955**, *97*.

(4) Verlet, L. *Phys. Rev.* **1967**, *159*.

(5) Bennett, C. In 1977; Chapter 5, pp 63–97.

(6) Chandler, D. *J. Chem. Phys.* **1978**, *68*, 2959–2970.

(7) Truhlar, D.; Garrett, B. *Acc. Chem. Res.* **1980**, *13*, 440–448.

(8) Kampen, N. V., *Stochastic Processes in Physics and Chemistry*; North-Holland: 1981.

(9) Swope, W.; Andersen, H.; Berens, P.; Wilson, K. *J. Chem. Phys.* **1982**, *76*.

(10) Berendsen, H.; Postma, J.; van Gunsteren, W.; et al. *J. Chem. Phys.* **1984**, *81*, DOI: https://doi.org/10.1063/1.448118.

(11) Car, R.; Parrinello, M. *Phys. Rev. Lett.* **1985**, *55*.

(12) Allen, M.; Tildesley, D., *Computer Simulation of Liquids*; Oxford University Press: 1987.

(13) Chandler, D., *Introduction to Modern Statistical Mechanics*; Oxford University Press: 1987.

(14) Hoover, W., *Computational Statistical Mechanics*; Elsevier: 1991.

(15) Natanson, G.; Garrett, B.; Truong, T.; Joseph, T.; Truhlar, D. *J. Chem. Phys.* **1991**, *94*, DOI: https://doi.org/10.1063/1.460123.

(16) Colvin, V.; Schlamp, M.; Alivisatos, A. *Nat.* **1994**, *370*, 354–357.

(17) Tolbert, S.; Alivisatos, A. *Sci.* **1994**, *265*, 373.

(18) Essmann, U.; Perera, L.; Berkowitz, M.; Darden, T.; Lee, H.; Pedersen, L. *J. Chem. Phys.* **1995**, *103*, 8577–8593.

(19) Tolbert, S.; Alivisatos, A. *J. Chem. Phys.* **1995**, *102*, 4642.

(20) Chen, C.; Herhold, A.; Johnson, C.; Alivisatos, A. *Sci.* **1997**, *276*, 398.

(21) Chan, W.; Nie, S. *Sci.* **1998**, *281*, 2016–2018.

(22) Chandler, D., *Barrier crossings: classical theory of rare but important events.* 1998, p 523.

(23) Dellago, C.; Bolhuis, P.; Chandler, D. *J. Chem. Phys.* **1998**, *108*.

(24) Landau, D.; Binder, K., *A Guide to Monte Carlo Simulation in Statistical Physics*; Cambridge University Press: 2000.

(25) Vlugt, T.; Dellago, C.; Smit, B. *J. Chem. Phys.* **2000**, *113*.

(26) Walters, P., *An Introduction to Ergodic Theory*; Springer-Verlag: 2000, pp 1–3.

(27) Jacobs, K.; Zaziski, D.; Scher, E.; Herhold, A.; Alivisatos, A. *Sci.* **2001**, *293*, 1803.

(28) Leach, A., *Molecular Modelling, Principles and Applications*, 2nd; Pearson: 2001.

(29) Bolhuis, P.; Chandler, D.; Dellago, C.; Geissler, P. *Ann. Rev. Phys. Chem.* **2002**, *53*, 291–318.

(30) Frenkel, D.; Smit, B., *Understanding Molecular Simulations*, 2nd; Academic: 2002.

(31) Jacobs, K.; Wickham, J.; Alivisatos., A. *J. Phys. Chem. B.* **2002**, *106*, 3759.

(32) Rabani, E. *J. Chem. Phys* **2002**, *116*, DOI: https://doi.org/10.1063/1.1424321.

(33) Dellago, C.; Bolhuis, P.; Geissler, P., *Transition Path Sampling*; John Wiley & Sons: 2003; Chapter 1, pp 1–78.

(34) Van Erp, T.; Bolhuis, P.; Moroni, D. *J. Chem. Phys.* **2003**, *118*, 7762–7774.

(35) Zaziski, D.; Prilliman, S.; Scher, E.; Casula, M.; Wickham, J.; Clark, S.; Alivisatos, A. *Nano. Lett.* **2004**, *4*, 943.

(36) Sowa, H. *Sol. Sta. Sci.* **2005**, *7*.

(37) Van Erp, T.; Bolhuis, P. *J. Comp. Phys.* **2005**, *205*, 157–181.

(38) Dellago, C.; Bolhuis, P.; Geissler, P., *Transition Path Sampling Methods*; Springer-Verlag Berlin Heidelberg: 2006, pp 351–389.

(39) Robel, I.; Subramanian, V.; Kuno, M.; Kamat, P. *J. Am. Chem. Soc.* **2006**, *128*, 2385–2393.

(40) Bussi, G.; Donadio, D.; Parrinello, M. *J. Chem. Phys.* **2007**, *126*.

(41) Van Erp, T. *Phys. Rev. Lett* **2007**, *98*.

(42) *Rare Event Simulation using Monte Carlo Methods*; Rubino, G., Tuffin, B., Eds.; John Wiley and Sons: 2009.

(43) Grünwald, M.; Dellago, C. In *Trends in Computational Nanomechanics. Challenges and Advances in Computational Chemistry and Physics.* Springer: 2010; Chapter Transition Path Sampling Studies of Solid-Solid Transformations in Nanocrystals under pressure.

(44) Kästner, J. *Int. Rev. Comp. Mol. Sci.* **2011**, *1*, 932–942.

(45) Hanwell, M.; Curtis, D.; Lonie, D.; Vandermeersch, T.; Zurek, E.; Hutchison, G. *J. Cheminf.* **2012**, *4*.

(46) Van Erp, T. *Adv. Chem. Phys.* **2012**, *151*.

(47) Abraham, M.; Murtola, T.; Schulz, R.; S.Pàll; Smith, J.; Hess, B.; Lindahl, E. *SoftwareX* **2015**, *1-2*, 19–25.

(48) Cabriolu, R.; Refsnes, K.; Bolhuis, P.; van Erp, T. *J. Chem. Phys.* **2017**, *147*, DOI: https://doi.org/10.1063/1.4989844.

(49) Riccardi, E.; Dahlen, O.; van Erp, T. *J. Phys. Chem. Lett.* **2017**, *8*, 4456–4460.

(50) Atkins, P.; de Paula, J.; Keeler, J., *Physical Chemistry*, 11th; Oxford: 2018.

(51) Wartha, E.; Bösenhofer, M.; Harasek, M. *Comb. Sci. Tech.* **2021**, *193*, 2087–2832.

(52) https://en.wikipedia.org/wiki/Transition_state_theory#/media/File:Rxn_coordinate_diagram_5.PNG.

(53) https://en.wikipedia.org/wiki/File:Saddle_point.png#filelinks.

(54) https://www.ipam.ucla.edu/programs/long-programs/complex-high-dimensional-energy-landscapes/.

(55) Lervik, A.; Svenum, I.; Wang, Z.; Cabriolu, R.; Riccardi, E.; Andersson, S.; van Erp, T.

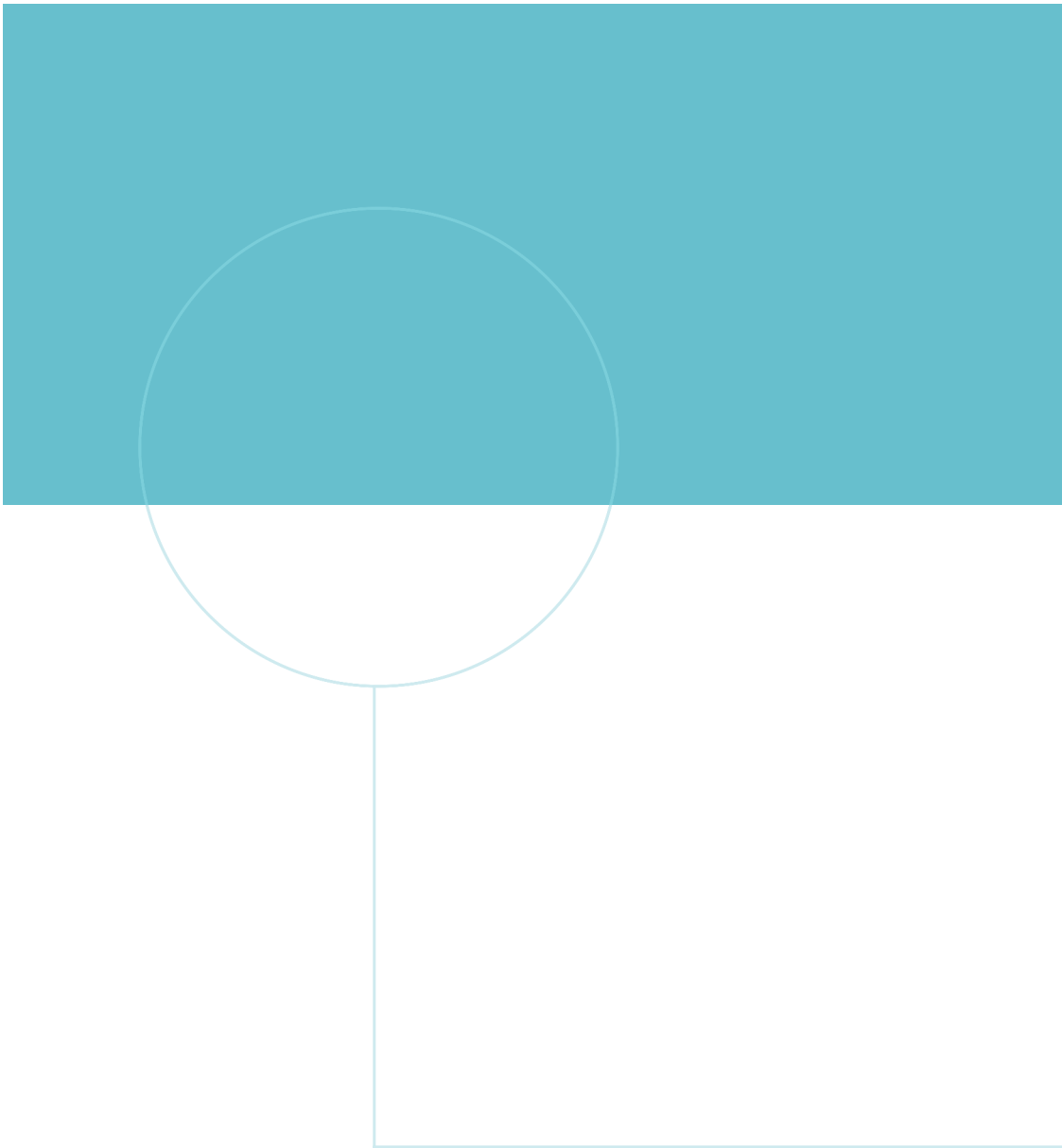

NTNU

Kunnskap for en bedre verden